JGR Atmospheres

RESEARCH ARTICLE
10.1029/2018JD029850

Key Points:
- Development and validation of a monthly, 0.1-degree ET_a data set (1982–2012) for China by the latest complementary relationship
- The new ET_a data require only basic meteorological variables and are more accurate than seven previously available ET_a products
- ET_a increased significantly in most parts of western and northeastern China, but opposite trends occurred in the North China Plain and eastern and southern China

Supporting Information:
- Supporting Information S1

Correspondence to:
N. Ma,
ningma@itpcas.ac.cn

Citation:
Ma, N., Szilagyi, J., Zhang, Y., & Liu, W. (2019). Complementary-relationship-based modeling of terrestrial evapotranspiration across China during 1982–2012: Validations and spatiotemporal analyses. *Journal of Geophysical Research: Atmospheres*, *124*. https://doi.org/10.1029/2018JD029850

Received 18 OCT 2018
Accepted 5 MAR 2019
Accepted article online 21 MAR 2019

Complementary-Relationship-Based Modeling of Terrestrial Evapotranspiration Across China During 1982–2012: Validations and Spatiotemporal Analyses

Ning Ma[1], Jozsef Szilagyi[2,3], Yinsheng Zhang[1,4], and Wenbin Liu[5]

[1]Key Laboratory of Tibetan Environment Changes and Land Surface Processes, Institute of Tibetan Plateau Research, Chinese Academy of Sciences, Beijing, China, [2]Department of Hydraulic and Water Resources Engineering, Budapest University of Technology and Economics, Budapest, Hungary, [3]Conservation and Survey Division, School of Natural Resources, University of Nebraska-Lincoln, Lincoln, NE, USA, [4]Center for Excellence in Tibetan Plateau Earth Sciences, CAS, Beijing, China, [5]Key Laboratory of Water Cycle and Related Land Surface Processes, Institute of Geographic Sciences and Natural Resources Research, Chinese Academy of Sciences, Beijing, China

Abstract Having recognized the limitations in spatial representativeness and/or temporal coverage of (i) current ground ET_a observations and (ii) land surface model- and remote sensing-based ET_a estimates due to uncertainties in soil and vegetation parameters, a calibration-free nonlinear complementary relationship (CR) model is employed with inputs of air and dew-point temperature, wind speed, and net radiation to estimate 0.1°, monthly ET_a over China during 1982–2012. The modeled ET_a rates were first validated against 13 eddy-covariance measurements, producing Nash-Sutcliffe efficiency values in the range of 0.72–0.94. On the basin scale, the modeled ET_a values yielded a relative bias of 6%, and a Nash-Sutcliffe efficiency value of 0.80 in comparison with water-balance-derived evapotranspiration rates across 10 major river basins in China, indicating the CR-simulated ET_a rates reliable over China. Further evaluations suggest that the CR-based ET_a product is more accurate than seven other mainstream ET_a products. The 31-year mean annual ET_a value decreases from the southeast to the northwest in China, resulting in a country average of 406 ± 15 mm/year. The country-representative annual ET_a rates slightly decreased with a rate of −0.5 mm/year ($p = 0.86$) during 1982–2012. Annual ET_a increased significantly over most parts of western and northeastern China but decreased significantly in many regions of the North China Plain as well as in the eastern and southern coastal regions. The present CR-based method, with its calibration-free nature and minimal data requirement, could help future calibrations/verifications of the more complex and more data-intensive land surface model- and remote sensing-based models.

1. Introduction

As a key component in global water and energy cycles (Wang & Dickinson, 2012), land surface evapotranspiration (ET_a) affects the climate via a wide range of feedbacks acting on air temperature, humidity, and precipitation (Shen et al., 2015; Shukla & Mintz, 1982; Teuling et al., 2010). Accurate estimation of ET_a is therefore fundamental not only to characterizing the effects of changing climate on the hydrological cycle but also to regional drought monitoring and water resources management (Fisher et al., 2017). However, quantifying ET_a remains a challenging task since it is controlled by complicated interactions among atmospheric demand, soil water status, and typically heterogeneous vegetation and soil properties (Jung et al., 2010; Or & Lehmann, 2019; Teuling et al., 2009; Wu et al., 2017).

The emergence of shared eddy-covariance (EC) ET_a observations during the past few years (e.g., FLUXNET; Baldocchi et al., 2001) has substantially advanced our knowledge of terrestrial evapotranspiration in various ecosystems. Unfortunately, however, the observation period of most EC flux towers is shorter than a decade, thus impeding the depiction of long-term variability in ET_a (see Figure 1 in Chu et al., 2017, for a detailed list of observational periods of the FLUXNET towers). Furthermore, the spatial distribution of the EC flux stations is uneven globally, with the majority of the stations operated in Europe and North America, having far fewer stations in Asia, South America, and Africa (Chu et al., 2017; Jung et al., 2010; Yu et al., 2006). Due to these difficulties, especially in developing countries, a need arises to develop robust estimates of large-scale

terrestrial evapotranspiration rates for a better understanding of land-atmosphere energy and water exchanges at the regional, continental, and/or global scales and also to detect variations in diverse components of the hydrological cycle due to the ongoing climate change.

For the purpose of mapping large-scale ET_a information, continuous progress has been made by the application of land surface models (LSMs; see, e.g., Dirmeyer et al., 2006; Ma et al., 2017; Rodell et al., 2004) and remote sensing (RS) models (Chen et al., 2014; Purdy et al., 2018; Yao et al., 2017), by spatial upscaling of site-level ET_a via the employment of empirical methods, such as machine learning algorithms (Jung et al., 2010; Wang et al., 2017; Xu et al., 2018), and by data assimilation systems (Peters-Lidard et al., 2011; Xu et al., 2011). All these led to a more thorough representation of ET_a variability at extended spatial (e.g., regional and global) and/or temporal scales (e.g., multiyear and decadal). At the same time, however, numerous evaluation studies showed that there exists a potentially high uncertainty up to the order of ~30% in such ET_a products (Bai & Liu, 2018; Baik et al., 2018; Jiménez et al., 2011; Liu, Wang, et al., 2016; Long et al., 2014; Miralles et al., 2016; Mueller et al., 2011; Sörensson & Ruscica, 2018; Velpuri et al., 2013), which stems primarily from uncertainties in the meteorological forcing, model physical structures, and/or parameter values (Badgley et al., 2015; Trambauer et al., 2014). Jiménez et al. (2011), for example, demonstrated that the uncertainties in global annual mean ET_a between different models and data sets may even reach 50%, indicating a great challenge in accurately representing large-scale ET_a across the world. It should be noted that the majority, if not all, of the above-mentioned ET_a models relies heavily on detailed surface vegetation (e.g., leaf area index, canopy height, and land cover/land use type) and soil (e.g., soil physical type, moisture status, porosity, layering, thickness, and rooting depth) information in order to have the models cover multiple biomes (e.g., Jung et al., 2010; Ma et al., 2017; Martens et al., 2017; Purdy et al., 2018). Additionally, days with large cloud cover create a stumbling block for RS of surface properties and so do sparsely vegetated areas where vegetation parameters cannot be well detected by satellites. For example, RS models still fail to provide ET_a information over approximately 15% of the total area of China where desert and sparse grassland regions meet (see, e.g., Figure 5 in Chen et al., 2014). Similarly, most state-of-the-art LSMs are also struggling for an appropriate dynamic vegetation module to fully represent plant transpiration processes, which then propagates errors in their modeled ET_a values, as has been highlighted by Ma et al. (2017). Other challenges in the parameterizations of various surface exchange coefficients (Chen & Zhang, 2009), storage and transmission of water through soil (Clark et al., 2015), and root water uptake (Warren et al., 2015) may also, to various extent, limit the ability of these LSMs to accurately depict ET_a. Note that in China, the soil data may also be uncertain due to relatively limited ground-based survey, which is especially true for the western and northern parts of the country (Shangguan et al., 2013), thus causing additional difficulties for using LSMs to simulate ET_a.

In recognition of the above challenges in estimating large-scale ET_a, an approach that dispenses with requiring land surface properties would be preferable, as some degree of uncertainty in vegetation and soil data is inevitable. Recent advances (Brutsaert, 2015; Szilagyi, 2018a; Szilagyi et al., 2017) in the complementary relationship (CR) of evapotranspiration (Bouchet, 1963) that builds on a feedback mechanism between ET_a and its potential maximum rate (ET_p) under the same environmental conditions provide an alternative way for estimating regional (i.e., on a scale larger than about 1 km) ET_a employing only standard meteorological measurements without the requirement of any information on vegetation and soil conditions. While the classical linear forms of the Complementary Relationship (e.g., the Advection-Aridity model of Brutsaert & Stricker, 1979, or the Complementary Relationship Areal Evapotranspiration model of Morton, 1983) have been extensively used to estimate ET_a at multiple spatial and temporal scales over the past decades (e.g., Crago & Crowley, 2005; Hobbins et al., 2001; Liu et al., 2006; Ma, Zhang, Szilagyi, et al., 2015; Ozdogan & Salvucci, 2004; Szilagyi, 2015; Szilagyi & Jozsa, 2008; Xu & Singh, 2005), Han et al. (2012) argued that a nonlinear formulation of the CR should be more appropriate because the linear version best performs under conditions that are neither extremely arid nor extremely wet. In this context, a recently developed nonlinear CR formulation by Brutsaert (2015) attracts increasing attention (Brutsaert et al., 2017; Hu et al., 2018; Liu, Liu, et al., 2016; Zhang et al., 2017). Subsequent modifications by Crago et al. (2016) and Szilagyi et al. (2017), with a revised physical constraint, further improved the skill of this nonlinear CR model in estimating ET_a over different climate conditions (Crago & Qualls, 2018; Szilagyi, 2018a, 2018b;

Szilagyi & Jozsa, 2018). The most prominent advantage in the Szilagyi et al. (2017) version of the CR is that it establishes the value of the Priestley-Taylor coefficient (Priestley & Taylor, 1972) by spatially integrating temperature and humidity data over wet areas. As such, the model avoids complex trial-and-error calibrations requiring prior information of "ground-truth" ET_a. This is important because regionally representative such ET_a data for calibration are often missing in developing countries, including China.

While a wide range of studies have investigated the spatiotemporal pattern of ET_a across China (Chen et al., 2014; Gao et al., 2007; Li, Liang, et al., 2014; Mao & Wang, 2017; Su et al., 2015; Sun et al., 2017; Yang et al., 2018), there exist considerable inconsistencies for both magnitudes and trends of ET_a due primarily to the uncertainties in parameters and/or forcing of different models. In the present study, by fully taking advantage of the recent improvements in the nonlinear CR model formulation, we aim to (1) develop a 31-year (1982–2012), 0.1° ET_a product across China, along with independent validations using plot-scale EC measurements and basin-scale water-balance-derived evapotranspiration rates; (2) determine whether this new CR-based ET_a product improves upon previously available ET_a products; and (3) quantify the spatial and temporal variability of ET_a in China during the past three decades.

2. Materials and Methods

2.1. Model Description

The Szilagyi et al. (2017) formulation of Brutsaert's (2015) nonlinear CR model was employed for large-scale ET_a simulation, which relates two dimensionless evapotranspiration terms such as

$$y = (2-X)X^2, \tag{1}$$

where y and X are defined as

$$X = \frac{ET_{pmax}-ET_p}{ET_{pmax}-ET_w}\frac{ET_w}{ET_p}, \tag{2}$$

$$y = \frac{ET_a}{ET_p}. \tag{3}$$

Here the ET_p potential evapotranspiration term describes the evapotranspiration rate of a small wet patch in a drying (i.e., not fully wet) environment, typically expressed by the Penman (1948) equation as

$$ET_p = \frac{\Delta(R_n-G)}{(\Delta+\gamma)} + \frac{\gamma f_u(e_o-e_a)}{(\Delta+\gamma)}, \tag{4}$$

where Δ (kPa/°C) is the slope of the saturation vapor pressure curve at air temperature, T_a (°C); γ is the psychrometric constant (kPa/°C). R_n and G are net radiation and soil heat flux into the ground in water equivalent of millimeters per day, respectively. e_o and e_a are the saturation and actual vapor pressure of the air (kPa), respectively. f_u is the wind function that includes the 2-m wind speed (U_2, m/s), that is,

$$f_u = 2.6\times(1+0.54U_2). \tag{5}$$

ET_w is the wet environment evapotranspiration rate, observed over a regionally extensive well-watered surface, specified by the Priestley-Taylor equation (Priestley & Taylor, 1972), that is,

$$ET_w = \alpha\frac{\Delta_{Twea}}{\Delta_{Twea}+\gamma}(R_n-G) \tag{6}$$

Note that equation (6) was derived for completely wet environments by Priestley and Taylor (1972), and therefore, Δ_{Twea} should be evaluated at the air temperature observed in a wet environment, T_{wea} (°C), instead of T_a (Szilagyi, 2014; Szilagyi & Jozsa, 2008). This is important since previous studies have found that the difference between these two may reach 2–10 °C (Ma, Zhang, Szilagyi, et al., 2015; Szilagyi, 2014). By

making use of a negligible vertical air temperature gradient observable in wet environments, T_{wea} can be approximated by the wet surface temperature, T_{wes} (°C). Szilagyi and Schepers (2014) demonstrated that the wet surface temperature is independent of areal extent, thus T_{wes} can be obtained from the Bowen ratio of a small wet patch for which the Penman equation is valid, that is,

$$\beta_{we} = \frac{R_n - G - ET_p}{ET_p} \approx \gamma \frac{T_{wes} - T_a}{e_{o,Twes} - e_a}, \tag{7}$$

in which β_{we} is the Bowen ratio of the well-watered patch (assuming that available energy for the wet patch is close to that of the drying surface), $e_{o,Twes}$ being the saturated vapor pressure at T_{wes} ($\approx T_{wea}$). Note that T_{wes} may be larger than T_a when the air is close to saturation, and in such cases, T_{wea} should be capped by T_a (Szilagyi, 2014; Szilagyi & Jozsa, 2018). α in equation (6) is the dimensionless Priestley-Taylor coefficient, with typical values from the range of [1.1–1.32] (Morton, 1983). For large-scale model applications when measured ET_a is lacking for the calibration of α, Szilagyi et al. (2017) proposed a novel method to find an appropriate value of α by identifying wet grid cells and utilizing observed gridded T_a and humidity data over them. The derived α value of 1.12 was used for the present country-scale simulation (see Appendix A for how it was derived for China).

ET_{pmax} is the maximum value that E_p can, in theory, reach, which may appear when the air loses all moisture, that is,

$$ET_{pmax} = \frac{\Delta_{Tdry}}{\Delta_{Tdry} + \gamma}(R_n - G) + \frac{\gamma}{\Delta_{Tdry} + \gamma} f_u \, e_{o,Tdry} \tag{8}$$

in which Δ_{Tdry} (kPa/°C) and $e_{o,Tdry}$ (kPa) are the slope of the saturation vapor pressure curve and the saturated vapor pressure, respectively, at the dry-environment air temperature, T_{dry} (°C). The latter can be estimated from the adiabat of an air parcel in contact with the drying surface under a constant available energy at the surface (Szilagyi, 2018a), that is,

$$T_{dry} = T_{wb} + \frac{e_{o,Twb}}{\gamma}, \tag{9}$$

where T_{wb} (°C) is the wet-bulb temperature and $e_{o,Twb}$ (kPa) is the saturated vapor pressure at T_{wb}. T_{wb} is derived by another iteration of solving for the Bowen ratio during adiabatic changes (Szilagyi, 2014), that is,

$$\gamma \frac{T_{wb} - T_a}{e_{o,Twb} - e_{o,Td}} = -1, \tag{10}$$

in which $e_{o,Td}$ (kPa) is the saturated vapor pressure at the dew-point temperature, T_d (°C).

2.2. Forcing Data

Meteorological forcing data from the China Meteorological Forcing Dataset (CMFD; available online http://westdc.westgis.ac.cn/data/7a35329c-c53f-4267-aa07-e0037d913a21), which was developed by the Data Assimilation and Modeling Center for Tibetan Multispheres of the Institute of Tibetan Plateau Research of the Chinese Academy of Sciences (He & Yang, 2011), were used to drive the CR model in the present study. It has near-surface air temperature (T_a), specific humidity (q), air pressure ($Pres$), 10-m wind speed (U_{10}), precipitation, and downward shortwave (DSR) and longwave (DLR) radiation with spatial and temporal resolutions of 0.1° and 3 hr, respectively, covering the period of 1979–2015 across China. The CMFD was constructed by merging in situ measurements at 740 China Meteorological Administration stations with advanced retrospective analyses data from (i) Global Land Data Assimilation System; (ii) GEWEX Surface Radiation Budget; and (iii) Tropical Rainfall Measuring Mission precipitation measurements (He & Yang, 2011). A wide range of validation studies suggest that CMFD shows a reasonable consistency with ground-measured meteorological data, demonstrating that it is a reliable gridded forcing in China (e.g., Chen et al., 2011; Zhou et al., 2015). It is therefore being widely used for not only driving the hydrological model and LSM (e.g., Ma et al., 2016; Sun et al., 2017) but also assessing the impacts of long-term climate change in China (e.g., Chu et al., 2015; Zhao et al., 2016).

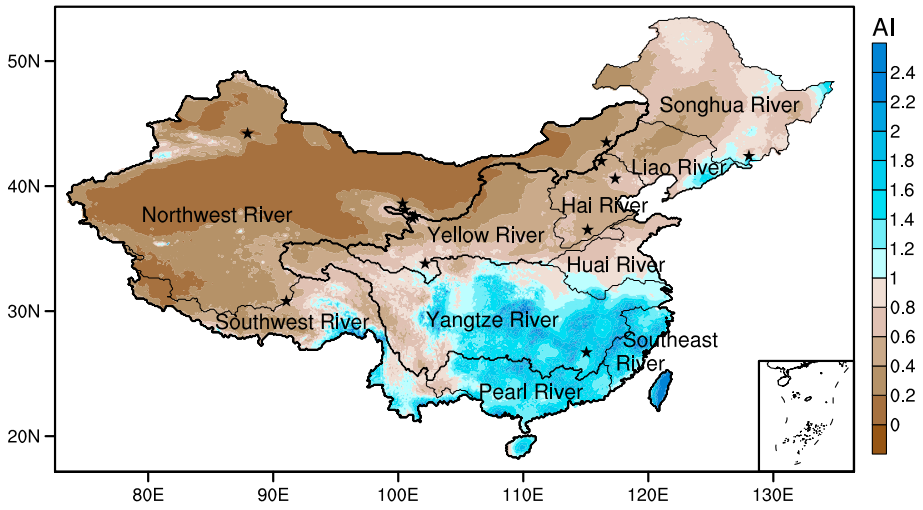

Figure 1. The geographical locations of the 13 eddy-covariance flux towers (filled stars) and the 10 major river basins in China. Overlain are the multiyear (1982–2012) mean annual aridity index (AI) values, that is, the ratio of annual precipitation to Penman potential evapotranspiration, to show the climatic background.

CMFD 10-m wind speed values were converted to 2-m values by $U_2 = U_{10}\,(2/10)^{1/7}$ (Brutsaert, 2005). The T_d values were derived from the *q* and *Pres* data of CMFD (Allen et al., 1998). We derived R_n (see Appendix B for details) with the help of *DSR* and *DLR* from CMFD, longwave broadband emissivity and albedo data from the Global Land Surface Satellite observations (GLASS; available online at http://glcf.umd.edu/data/; Liang et al., 2013), and land surface temperature (*LST*) data from Moderate Resolution Imaging Spectroradiometer (MODIS, available online at https://modis.gsfc.nasa.gov/data/dataprod/mod11.php; Wan, 2014). Since *G* is usually considered to be a small proportion of R_n due to a typical lack of large-scale measurements of soil heat fluxes (Brutsaert, 2005), it was assumed to approximately equal 5% of R_n (Kustas et al., 1993). All forcing data (i.e., T_a, T_d, R_n, and U_2) were averaged for the given month at a spatial resolution of 0.1°, thereby driving the CR model (equation (1)) during 1982–2012 at a monthly time step across China.

2.3. Validation Data Sets

2.3.1. EC Measured Actual Evapotranspiration

EC measurements of actual evapotranspiration ($ET_{a\text{-}mea}$) came from 13 flux stations within the ChinaFLUX (Yu et al., 2006; available online http://www.chinaflux.org/), WATER (Li et al., 2009; available online http://westdc.westgis.ac.cn/water/), Haihe Experiments (Liu et al., 2013; available online http://westdc.westgis.ac.cn/haihe), and FLUXNET (Baldocchi et al., 2001; available online http://fluxnet.fluxdata.org/) programs to validate the CR-simulated ET_a values. With annual precipitation ranging from 150 to 1,542 mm, these EC stations are located in a wide range of climate zones, covering China's major terrestrial ecosystems including forests, croplands, shrublands, meadows, steppe, and desert. Figure 1 illustrates the spatial distribution of the flux stations, while Table 1 lists detailed information for these 13 EC stations.

The EC-measured latent heat fluxes (λE) in nine stations are 30-min values with partial gaps due primarily to extreme weather and/or sensor failures. We first applied the marginal distribution sampling technique (Reichstein et al., 2005) to fill these half-hourly gaps and subsequently aggregated the so-derived values into monthly $ET_{a\text{-}mea}$ for validation purposes. At the remaining four stations, including Maqu, Fukang, Duolun, and Haibei-M, any gaps in λE were filled by the original principle investigators. In total, 264 site-months $ET_{a\text{-}mea}$ data were employed to validate the modeled results in the present study. Note that the footprints of the EC-measured fluxes (~0.3–1 km) are generally smaller than the area of the model grid in the present study (~11 km). Any heterogeneity within the grid cell is assumed negligible, thereby neglecting the subgrid scale variations of ET_a. By doing so, the ET_a values of the grid cells in which the flux towers are found are directly compared to the EC measurements during the same periods.

Table 1
Basic Information for the 13 Eddy-Covariance Flux Stations Employed in This Study

Station name	Latitude, longitude, elevation	Land cover type	Climate	MAP	Period	References
Arou	38.04°N, 100.46°E, 3,033 m	Meadow	Alpine	405	2009	M. Ma et al. (2008)
Changbaishan	42.40°N, 128.09°E, 738 m	Mixed forest	Temperate	713	2003–2005	J. Wu et al. (2013)
Dangxiong	30.50°N, 91.07°E, 4,333 m	Meadow	Alpine	450	2005	Shi et al. (2006)
Duolun	42.05°N, 116.28°E, 1,350 m	Steppe	Temperate	399	2006–2007	S. Chen et al. (2009)
Fukang	44.28°N, 87.93°E, 475 m	Desert	Temperate	150	2004	R. Liu et al. (2012)
Guantao	36.52°N, 115.13°E, 30 m	Cropland	Temperate	528	2008–2010	S. Liu et al. (2013)
Guantan	38.53°N, 100.25°E, 2,835 m	Forest	Subalpine	435	2010	X. Li et al. (2009)
Haibei-S	37.67°N, 101.33°E, 3,358 m	Shrub	Alpine	570	2003	L. Zhao et al. (2006)
Haibei-M	37.60°N, 101.33°E, 3,250 m	Meadow	Alpine	561	2002–2003	Kato et al. (2006)
Maqu	33.89°N, 102.14°E, 3,423 m	Meadow	Alpine	593	2010	Shang et al. (2015)
Miyun	40.63°N, 117.32°E, 350 m	Orchard	Temperate	489	2008–2010	S. Liu et al. (2013)
Neimengu	43.55°N, 116.68°E, 1,200 m	Steppe	Temperate	350	2005	Hao et al. (2007)
Qianyanzhou	26.74°N, 115.06°E, 102 m	Coniferous forest	Subtropical	1,542	2003–2004	Wen et al. (2006)

Note. MAP = multiyear mean annual precipitation (mm/year).

2.3.2. Basin-Scale Water-Balance-Derived Actual Evapotranspiration

At a basin (or larger) scale, the water-balance method of employing precipitation, runoff, and changes in terrestrial water storage is usually regarded as the most accurate way for estimating ET_a, though it cannot depict the spatial variability of ET_a within the basin. Terrestrial evapotranspiration rates for 10 major river basins in China were derived by the water-balance-based method, assuming any interbasin groundwater exchange as negligible (Liu, Wang, et al., 2016; Zeng et al., 2014), that is,

$$ET_{wb} = P - Q - \Delta S, \tag{11}$$

where ET_{wb} is the annual basin-scale actual evapotranspiration rate from the water-balance method. P, Q, and ΔS are precipitation, runoff, and changes in terrestrial water storage for a given basin, respectively. Although most studies assume ΔS negligible at an annual scale, recent works discussed the importance of ΔS in estimating ET_{wb} with equation (11) (Han et al., 2015; Liu, Wang, et al., 2016; Zeng et al., 2014). Therefore, the Gravity Recovery and Climate Experiment (GRACE) measurements were (see below) included in equation (11) in order to reduce the uncertainties in the annual ET_{wb} estimates.

2.3.2.1. Annual Precipitation and Runoff Data in 10 Major River Basins of China

To provide a national standard for water resource management and regulations, the Ministry of Water Resources of China divides the country into 10 level-I, 80 level-II, and 213 level-III water resources regions, based upon various river systems and/or administrative divisions. The level-I water resources regions maintain the integrity of the 10 major river basins in China, which include the Songhua, Liao, Hai, Yellow, Huai, Yangtze, Southeast, Pearl, and Southwest and Northwest River Basins (Figure 1). The drainage areas of these basins range from 24.5×10^4 to 336.2×10^4 km^2. The National Water Resources Bulletin, officially released by the Ministry of Water Resources in China, records the basin-wide annual precipitation (P) and runoff (Q) over these major river basins at an annual scale (available online http://www.mwr.gov.cn/sj/tjgb/szygb/). Since this data set is based on the official ground precipitation and runoff observation networks of the Ministry of Water Resources of China, it is regarded as the most accurate Chinese water resources statistics and has therefore been widely used for not only identifying long-term water resources variability (Li, Cao, et al., 2014; Piao et al., 2010) but also evaluating various ET_a products (Yang et al., 2018). Recently, Mao et al. (2016) quantified that the difference in the country-wide mean annual precipitation rate is only 7.5 mm between two data sources, that is, the Ministry of Water Resources and the China Meteorological Administration, suggesting that the former data source is indeed reliable. Limited by data availability, annual P and Q values over the 10 major river basins of China were employed for the 2004–2012 period in the present study, in combination with GRACE-measured ΔS, for the estimation of annual ET_{wb} by equation (11) for the same period and for each river basin.

2.3.2.2. GRACE Observations of ΔS

The basin-scale ΔS in this study was derived using GRACE-observed terrestrial water storage anomaly products (Tapley et al., 2004; available online http://grace.jpl.nasa.gov), which are released by three processing

Table 2
Overview of the Eight ET_a Products Employed in This Study

ET_a products	Category	Spatial resolution	Temporal resolution	References
FLUXNET-MTE	Upscaling of EC measurements	0.5° × 0.5°	Monthly	Jung et al. (2011)
ERA-Interim	Reanalysis	T255 (~79 km)	6 hr, monthly	Dee et al. (2011)
JRA-55	Reanalysis	1.25° × 1.25°	3 hr, daily, monthly	Kobayashi et al. (2015)
Noah	Land surface model	0.25° × 0.25°	3 hr, monthly	Beaudoing and Rodell (2015)
CLM	Land surface model	1° × 1°	3 hr, monthly	Rodell and Beaudoing (2007)
CLSM	Land surface model	0.25° × 0.25°	Daily	B. Li et al. (2018)
GLEAM	Remote sensing model	0.25° × 0.25°	Daily	Martens et al. (2017)
PML	Remote sensing model	0.5° × 0.5°	Monthly	Y. Zhang et al. (2016)

Note. Data coverage is 1982–2012 except for FLUXNET-MTE which terminated in 2011. EC = eddy-covariance; MTE = model tree ensemble; JRA-55 = Japanese 55-year reanalysis; CLM = Community Land Surface Model; CLSM = Catchment Land Surface Model; GLEAM = Global Land Evaporation Amsterdam Model; PML = Penman-Monteith-Leuning model.

centers: GeoforschungsZentrum Potsdam; Center for Space Research at University of Texas, Austin; and Jet Propulsion Laboratory; all based on the same Earth's gravity field. First, the published values were multiplied by the gain factors in each grid to restore the attenuated (due to the destriping, Gaussian, and degree-60 filters) signals to the land grids of each product (Landerer & Swenson, 2012). Then the arithmetic average of these three products was used to reduce the uncertainties due to the noise terms in the different solutions. Because the temporal resolution of GRACE is monthly, we considered the annual ΔS values for 2004–2012 as the difference in terrestrial water storage anomaly between successive Decembers.

2.4. Typical Long-Term ET_a Products

As there are numerous ET_a products available for both the hydrological and atmospheric communities (Jiménez et al., 2011; Mueller et al., 2011), it is necessary to compare the CR-simulated ET_a values' performance to other currently available ET_a models. Eight products were selected based on two criteria, that is, (i) the temporal coverage must be at least 30 years starting in the 1980s, and (ii) the products be derived by current mainstream methods, including LSM- and RS-based ones, reanalysis, as well as by empirical upscaling of EC flux towers. These include the following.

(1) FLUXNET- model tree ensembles (MTE) is a global EC measurement upscaling product of ET_a using a machine learning technique called MTE (available online https://www.bgc-jena.mpg.de/geodb/projects/Home.php; Jung et al., 2011). The MTE was first trained with measured flux data of 198 FLUXNET towers across a wide range of biomes worldwide; then ET_a is generated using the meteorological, land cover, and RS-derived fraction of absorbed photosynthetic active radiation data.

Reanalysis ET_a from (2) ERA-Interim (available online https://www.ecmwf.int/en/forecasts/datasets/archive-datasets/reanalysis-datasets/era-interim) of the European Centre for Medium-Range Weather Forecasts (Dee et al., 2011) and (3) Japanese 55-year reanalysis (JRA-55, available online http://jra.kishou.go.jp/JRA-55/index_en.html#jra-55) of the Japan Meteorological Agency (Kobayashi et al., 2015). ERA-Interim and JRA-55 are usually regarded as the state-of-the-art reanalysis data since both products are based on the most advanced four-dimensional variational data assimilation technique.

LSM-based ET_a products generated by (4) Noah (Chen & Dudhia, 2001); (5) the Community LSM (CLM; Oleson et al., 2013); and (6) the Catchment LSM (CLSM; Koster et al., 2000) from the Global Land Data Assimilation System Version 2 (Rodell et al., 2004; available online https://disc.gsfc.nasa.gov/datasets?keywords=GLDAS).

RS-based ET_a from (7) the Global Land Evaporation Amsterdam Model (GLEAM; available online https://www.gleam.eu/#home; Martens et al., 2017) and (8) the Penman-Monteith-Leuning (PML) model driven by gridded meteorological forcing and satellite vegetation parameters (available online https://data.csiro.au/dap/landingpage?pid=csiro:17375&v=2&d=true; Zhang et al., 2016). See Table 2 for additional information about these eight ET_a products. Readers are suggested to refer to the original references of the corresponding ET_a products for a thorough introduction.

2.5. Model Performance Evaluation Metrics and Statistical Methods

For statistics, the Pearson correlation coefficient (R), the root-mean-square error (RMSE), the relative bias, and the Nash-Sutcliffe efficiency (NSE) criterion were applied to evaluate modeled ET_a against the ground-truth EC flux tower measurements and the water-balance derived basin-scale ET_{wb} values.

For identifying long-term tendencies, linear trend functions were fit to the annual/seasonal ET_a values using the least-squares regression technique. Student's t test was employed to assess the statistical significance of the trends and only those with a p value less than 0.05 were considered as statistically significant.

3. Results

3.1. Model Validations

3.1.1. Validation Against Plot-Scale EC-Measured Actual Evapotranspiration Rates

The CR-simulated actual evapotranspiration rates were first validated against EC measurements ($ET_{a\text{-}mea}$) of 13 flux towers in China at a monthly scale (Figure 2). The CR model is able to capture both magnitude and phase of the monthly ET_a signal in all terrestrial biomes, as evidenced by the NSE values from the range of 0.72–0.94. The correlation coefficient values are all larger than 0.90 and are statistically significant at the $p = 0.001$ level (Figure 2). The RMSE values range from 4.9 to 16.2 mm/month with the minimum found at Fukang and the maximum at Dangxiong. To investigate the model's skill in reproducing the seasonal variability, another sort of NSE values using the mean seasonal cycle (instead of the average of monthly values) of $ET_{a\text{-}mea}$ as a benchmark were also calculated for each station (see the numbers in parentheses of Figure 2). It can be seen that such NSE values are almost positive except for Neimenggu station, indicating that the CR model is able to capture the seasonal variability of ET_a in the majority of stations.

Specifically, the model performs particularly well at the grassland sites (e.g., Arou, Maqu, Neimenggu, Haibei-M, and Haibei-S) except Dangxiong and Duolun, where ET_a rates were slightly overestimated and underestimated, respectively, leading to lower NSE values (0.78 and 0.72, respectively). The modeled ET_a values are also consistent with measurements at the desert Fukang site (NSE = 0.91) where the ground is rarely covered by vegetation. At the agricultural sites, Miyun and Guantao, the model was capable of reproducing the EC-measured rates with NSE values of 0.90 and 0.82, respectively. The modeled ET_a generally compares well with measurements at the three forest sites, that is, Changbaishan, Qianyanzhou, and Guantan, where all NSE values are higher than 0.86. These site-by-site comparisons demonstrate that the present calibration-free CR model adopted in this study is robust across a wide range of terrestrial ecosystems with different climates and land covers in China.

3.1.2. Validation Against Basin-Scale Water-Balance-Derived Evapotranspiration Data

Annual ET_{wb} values of 10 major river basins during 2004–2012, derived from precipitation, runoff, and changes in terrestrial water storage using equation (11), were further employed to assess the skill of the current CR model at a basin scale. Over the 10 major river basins in China, the simulated ET_a values follow closely the annual ET_{wb} rates during 2004–2012, illustrated by an NSE value of 0.80 and a relative bias of only 6% (Figure 3a). The values scatter almost perfectly around the 1:1 line of the regression plot with a best-fit line (not shown) of $ET_a = 0.968ET_{wb} + 42.3$, yielding an R value of 0.918 and a RMSE value of 76.9 mm/year, demonstrating that the calibration-free CR model reproduces ET_a successfully over multiple basins of China.

In an interbasin comparison of the 9-year averaged (2004–2012) basin-scale ET_a rates (Figure 3b), the CR model performs well in most river basins (relative biases are typically within ±10%) except for the Hai and Yangtze River Basins where actual evapotranspiration was underestimated by −12% and overestimated by 13%, respectively. The largest discrepancy, however, appears in the Southwest River Basin where ET_a from CR is ~580 mm/year, whereas ET_{wb} yields only about 400 mm/year. Note that the Southwest River Basin consists of a few large rivers (e.g., the Mekong River, the Salween River, and the Yarlung Zangbo River) that originate in the highest part of the Tibetan Plateau having the most varied topography in the world where a great amount of global-warming-induced glacier melting augments the surface-runoff rate (Immerzeel et al., 2010). Such a component of (i) snow accumulation and melting, however, may not be accurately accounted for in the GRACE-derived ΔS term of equation (11), and also (ii) precipitation rates in high altitudes (e.g., the Himalayas and the Hengduan Mountains) may be seriously underestimated by available measurements of typical valley locations for the presently derived ET_{wb} values. It is therefore

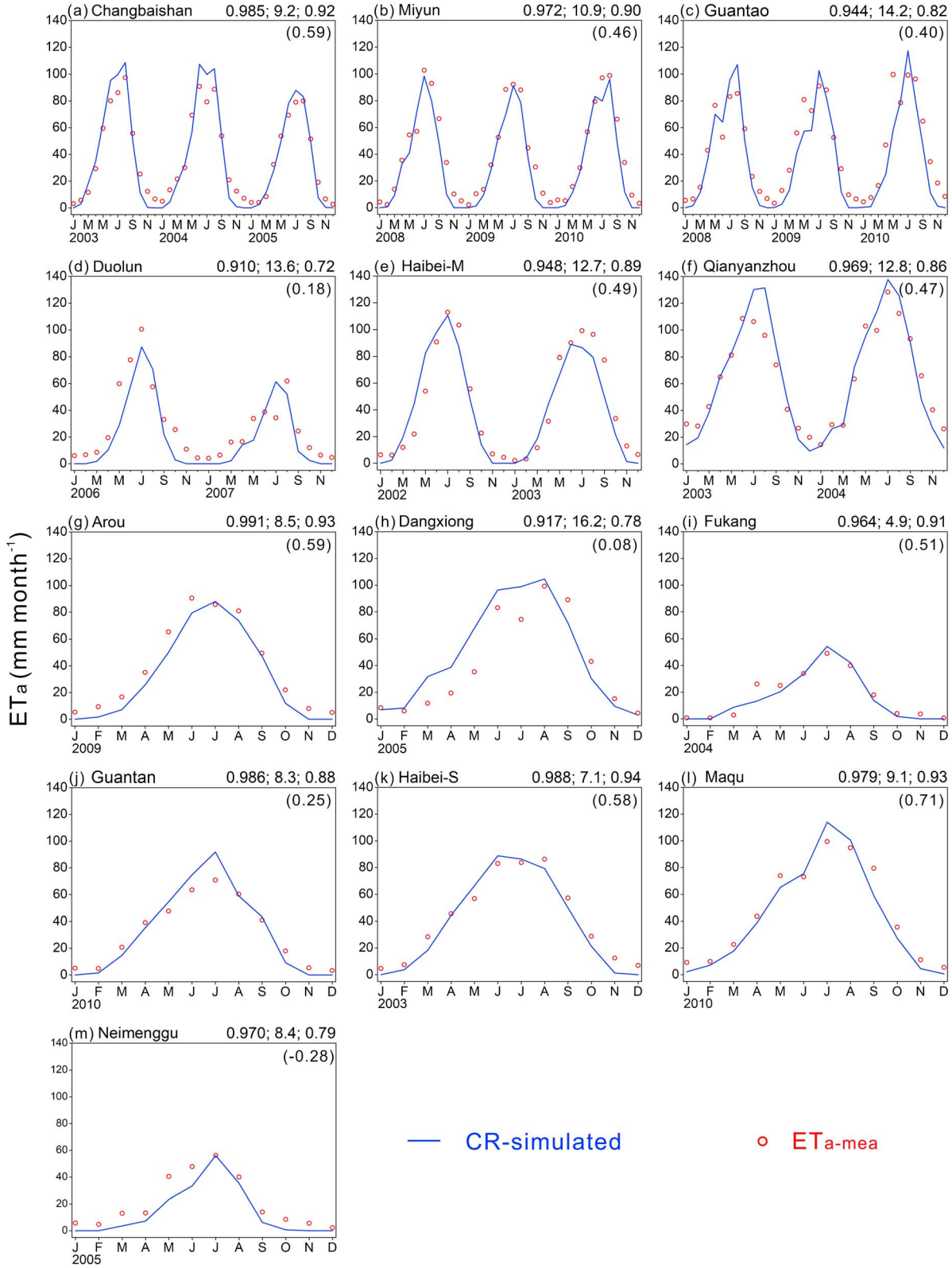

Figure 2. CR-simulated and eddy-covariance-measured ($ET_{a\text{-}mea}$) monthly evapotranspiration (ET_a) rates from the 13 flux stations (a–m) in China in years when the latter measurements were available. On the top of each panel, the model performance metrics are as follows: Pearson correlation coefficient (R), root-mean-square error (mm/month), and Nash-Sutcliffe efficiency. The number in the parentheses of each panel is another sort of Nash-Sutcliffe efficiency value calculated using the mean seasonal cycle of $ET_{a\text{-}mea}$ as a benchmark. CR = complementary relationship.

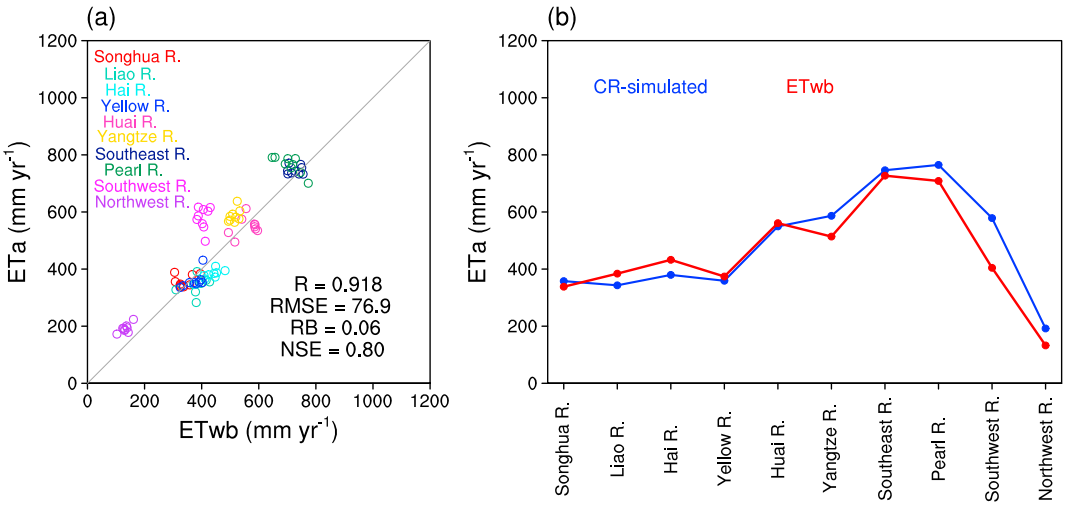

Figure 3. (a) Regression-plot of annual CR-simulated evapotranspiration rates (ET_a) and water-balance derived evapotranspiration (ET_{wb}) rates for the period of 2004–2012 and (b) their 9-year averaged values for the 10 major river basins in China. RMSE is in millimeters per year. CR = complementary relationship; R = Pearson correlation coefficient; RMSE = root-mean-square error; RB = relative bias; NSE = Nash-Sutcliffe efficiency.

believed that the actual evapotranspiration rate in the Southwest River Basin should be significantly higher than the water-balance derived 400-mm/year value.

3.2. Does the Present CR Approach Improve Existing ET_a Estimates Across China?

To explore whether the CR-simulated ET_a values are more accurate than those available from previous ET_a products, eight other widely available ET_a estimates were also evaluated against the water-balance-derived annual ET_{wb} values over the 10 major river basins in China for the 2004–2012 period (Figure 4). While ET_a from every product correlate statistically significantly with ET_{wb} (all $p < 0.001$), the resulting RMSE and NSE values vary to a large extent. In particular, the two reanalysis products, ERA-Interim and JRA-55, remarkably overestimate ET_a in all river basins with relative biases reaching 42% and 36%, respectively, leading to negative NSE values of −0.49 and −0.05, respectively. This is in accordance with a recent worldwide assessment of ET_a products against water-balance data by Liu, Wang, et al. (2016), which also demonstrated that the RMSE values of reanalysis products are much larger than other types of ET_a products. Among the three LSM-based products, Noah and CLSM tend to overestimate ET_a in humid river basins (e.g., CLSM reaches >1,000 mm/year, while ET_{wb} is only about 800 mm/year for the Southeast and Pearl River Basins), but such errors are much smaller in CLM (Figure 4). The positive biases in humid river basins are also apparent for FLUXNET-MTE, GLEAM, and PML, though they overall show good agreement with ET_{wb} in drier basins. Specifically, both GLEAM and PML overshoot ET_a in the Pearl, Southeast, and Yangtze River Basins by ~25% in comparison to ET_{wb}, leading to NSE values of 0.36 and 0.27, respectively.

By comparing Figures 3 and 4, it can be seen that the CR-modeled ET_a product has apparently higher NSE and lower RMSE and relative bias values than other seven products in China. That is, only CLM performs better than CR with higher NSE (=0.89) and lower RMSE (=57.9 mm/year) values. The improvement in the present CR-based ET_a product is not the result of a better spatial resolution (i.e., 0.1°). Notice the coarse resolution of the CLM ET_a product (1°), which impedes a detailed representation of a heterogeneous terrestrial biosphere. Further investigations, however, reveal erroneous CLM ET_a values for 1996 and 1997 when ET_a is seriously underestimated in most parts of China (see supporting information Figure S1), degrading CLM's ability to capture long-term variability of ET_a. Note also that CLM represents the landscape using patches of plant functional types instead of biomes within each modeling grid (Bonan et al., 2002), allowing the model to use more detailed optical, morphological, and physiological parameters derived from high-resolution satellite data. The soil inputs including soil color and organic content were also updated for a more reasonable parameterization of soil hydraulic and thermal conductivities (Lawrence et al., 2011). As a result, CLM could represent the water transfer through the soil-plant-atmosphere continuum better by

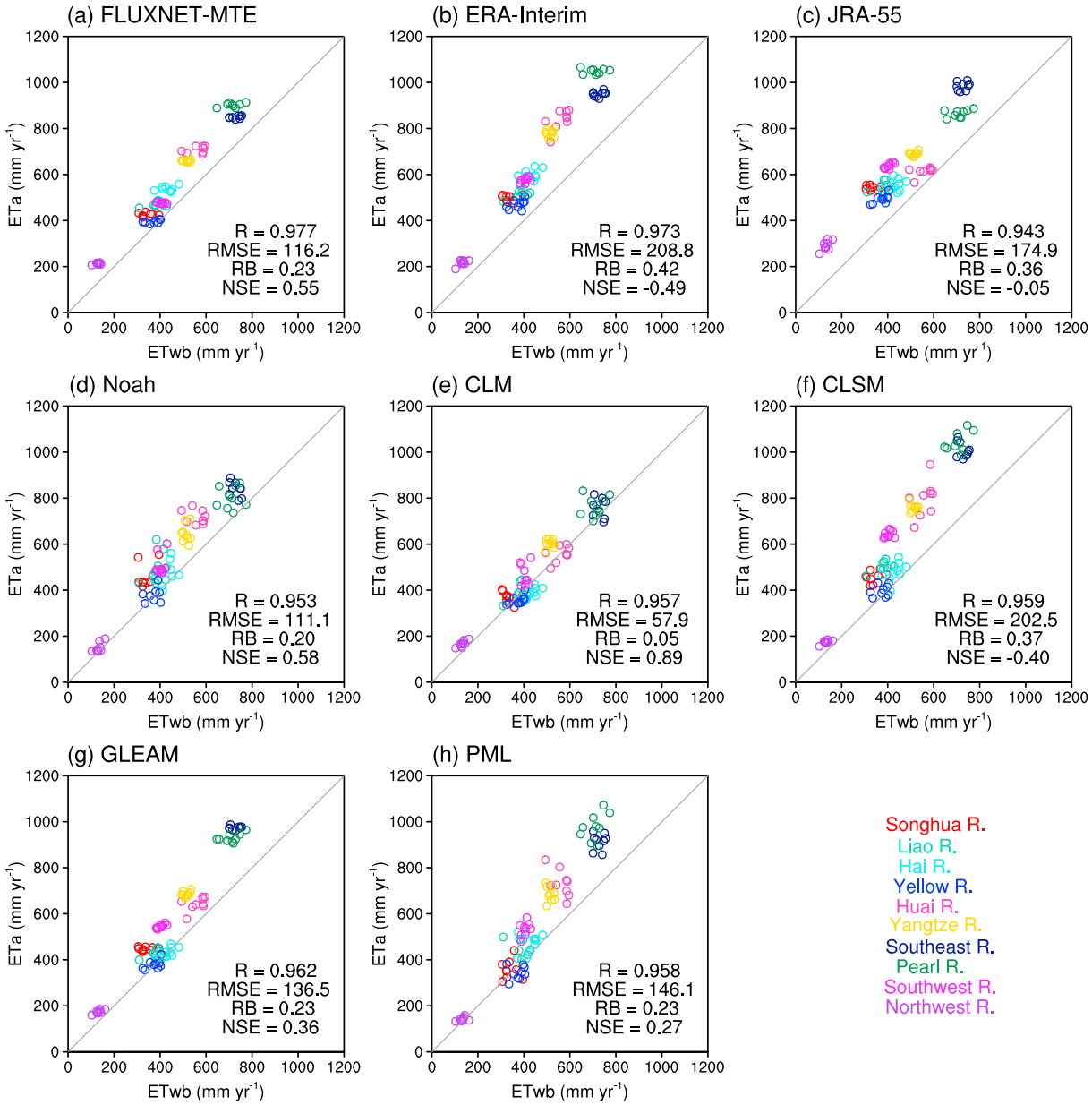

Figure 4. Annual evapotranspiration rates (ET_a) of (a) FLUXNET-MTE; (b) ERA-Interim; (c) JRA-55; (d) Noah; (e) CLM; (f) CLSM; (g) GLEAM, and; (h) PML plotted against the water-balance derived evapotranspiration (ET_{wb}) values for the 10 major river basins in China during 2004–2012. RMSE is in millimeters per year. R = Pearson correlation coefficient; RMSE = root-mean-square error; RB = relative bias; NSE = Nash-Sutcliffe efficiency; MTE = model tree ensemble; JRA-55 = Japanese 55-year reanalysis; CLM = Community Land Surface Model; CLSM = Catchment Land Surface Model; GLEAM = Global Land Evaporation Amsterdam Model; PML = Penman-Monteith-Leuning model.

its more detailed vegetation and soil parameters which may also explain the highest NSE value among the models considered here. Nevertheless, the present CR model does not need any additional vegetation or soil data required by LSMs- and RS-based models, providing a convenient avenue to obtain ET_a information over the data-scarce regions of the world.

3.3. Spatial Pattern of ET_a

3.3.1. Annual ET_a

In general, the multiyear (1982–2012) mean annual ET_a from the CR model decreases from the southeast to the northwest in China (Figure 5a), with the maximum value in excess of 1,200 mm/year in the Hainan Island and the minimum value less than 100 mm/year in the southern Xinjiang and western Inner

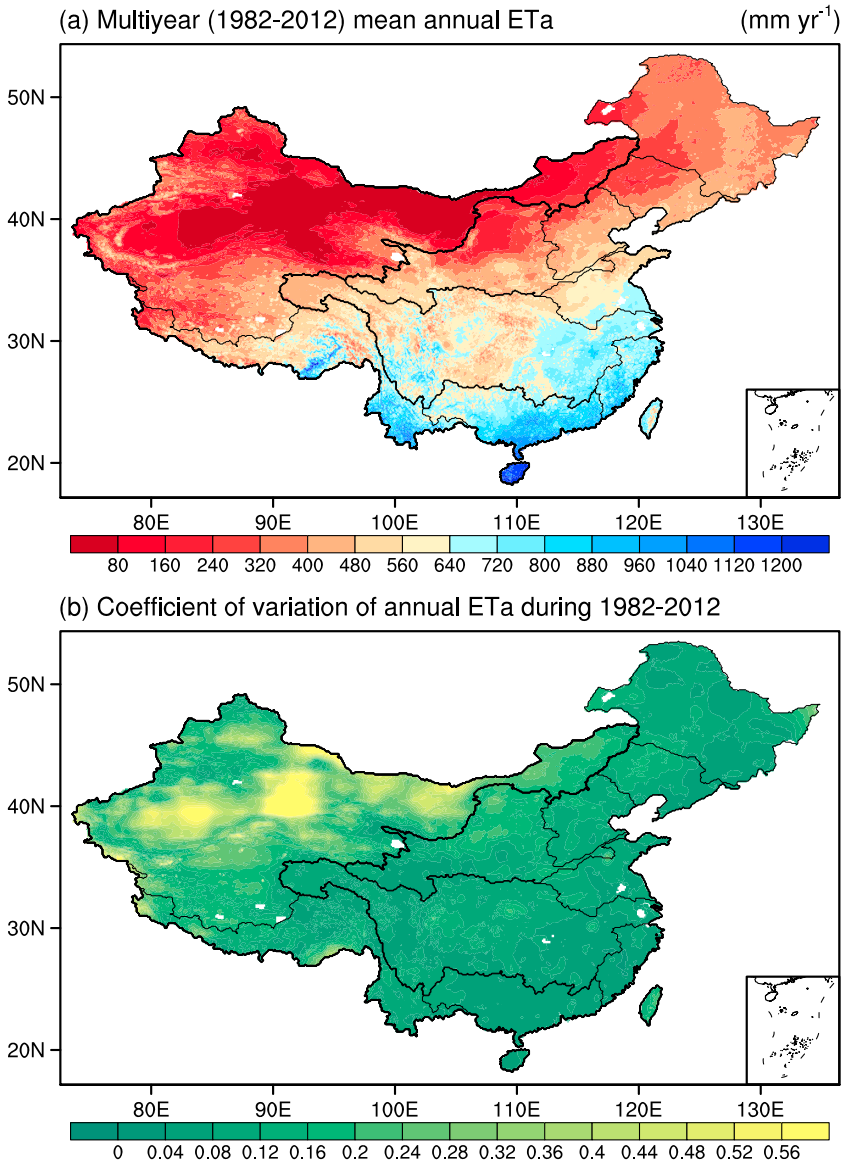

Figure 5. Spatial patterns of the complementary relationship-modeled (a) multiyear (1982–2012) mean annual ET_a and (b) coefficient of variation for the annual values.

Mongolia. ET_a reaches more than 1,000 mm/year in the Chinese southern coastal regions, dropping to approximately 800 mm/year in the south side of the Yangtze River. In Central China and the North China Plain, ET_a ranges from 400 to 650 mm/year while drops to less than 400 mm/year over large swaths of Inner Mongolia and northwestern China. Over the Tibetan Plateau where the elevation is typically higher than 3,500 m above sea level, ET_a also decreases from the southeastern to the northwestern Tibetan Plateau region, with values higher than 1,000 mm/year in the Brahmaputra Grand Canyon but lower than 240 mm/year in the Ngari. In general, the spatial pattern of annual ET_a simulated by the CR model follows that of the annual aridity index, a combined effect of atmospheric demand and water supply, showing a transition of humid to arid from the southeastern to the northwestern region of China. On the whole, the country-wide 31-year (1982–2012) mean annual CR-simulated ET_a over China is 406 ± 15 mm/year (mean ± standard deviation), with a coefficient of variation value of 0.037 (Figure 5b). The coefficient of variation is relatively high in northwestern China with a dry climate but becomes much smaller in eastern and southern China with a humid climate.

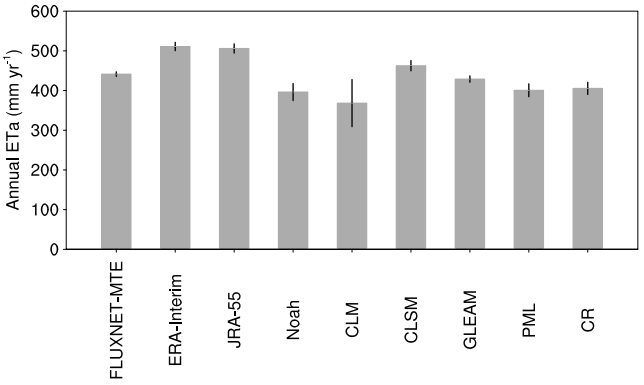

Figure 6. Comparison of the country-averaged multiyear mean annual ET_a rates in China from the CR and eight other models. Time span for calculating the mean value is 1982–2012 except for FLUXNET-MTE which ends in 2011. Error bar represents the interannual variability of the modeled values. MTE = model tree ensemble; JRA-55 = Japanese 55-year reanalysis; CLM = Community Land Surface Model; CLSM = Catchment Land Surface Model; GLEAM = Global Land Evaporation Amsterdam Model; PML = Penman-Monteith-Leuning model; CR = complementary relationship.

The spatial distribution of annual ET_a from the CR model also resembles those from other eight ET_a products (Figure S2). The country-averaged multiyear mean annual ET_a rate from the CR model is close to those from Noah (396 ± 22 mm/year) and PML (401 ± 16 mm/year) during the same period but slightly less than those of GLEAM (429 ± 8 mm/year) and FLUXNET-MET (441 ± 6 mm/year; Figure 6). Since FLUXNET-MTE does not contain ET_a for the nonvegetated areas in northwestern China (Figure S2), its multiyear mean annual value would be lower if such arid areas were included. It is also widely known that most explanatory variables employed to train the MTE were assumed static over the years, causing an underestimated interannual variance in the FLUXNET-MTE product (Jung et al., 2011). Note that the value of CLM in Figure 6 is probably questionable due to, as mentioned above, its problematic estimates in 1996 and 1997 (see Figures S1 and S3). Both reanalysis products (ERA-Interim with 511 ± 11 mm/year and JRA-55 with 506 ± 12 mm/year) yield much higher annual ET_a rates than that of CR, thus can be considered unrealistic based on the above water-balance-based evaluations.

3.3.2. Seasonal ET_a

Figure 7 illustrates the multiyear mean spring (March, April, and May), summer (June, July, and August), autumn (September, October, and November), and winter (December, January, and February) ET_a across China. Spatially, the seasonal ET_a in spring, summer, and autumn displays a geographical distribution pattern comparable with that of annual ET_a; however, in winter, its zonal characteristics become unclear as a

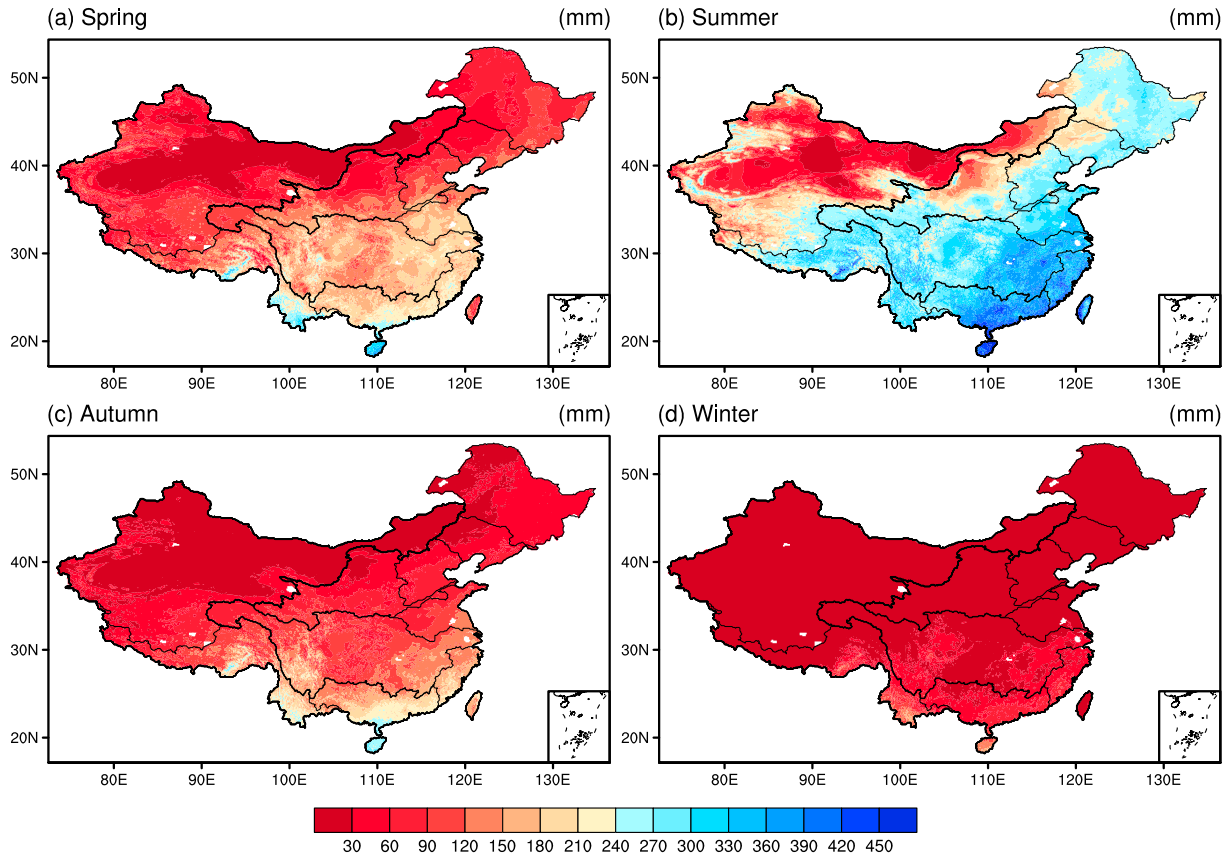

Figure 7. Spatial patterns of the complementary relationship-modeled multiyear (1982–2012) mean seasonal ET_a values (mm per season) across China; (a) spring, (b) summer, (c) autumn, and (d) winter.

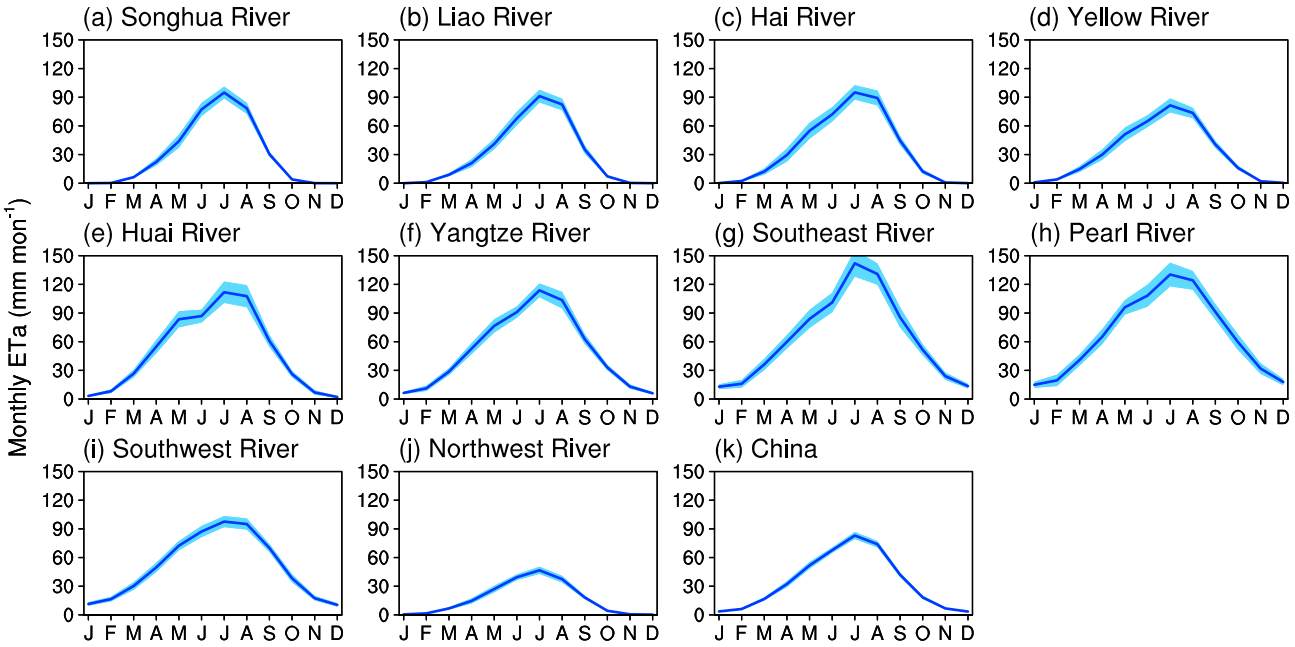

Figure 8. The multiyear (1982–2012) mean annual cycle of ET_a by the complementary relationship model over (a–j) the 10 major river basins plus over (k) China. The shaded area (light blue) represents the standard deviation of the modeled ET_a to indicate the interannual variability for each month of the year.

result of an overall minima in precipitation and available energy (Figure 7d). While summer ET_a is still lower than 100 mm in most parts of northwestern China because of the scarce precipitation in the region, it reaches 230–320 mm in northeastern China and the North China Plain, increasing to more than 380 mm in most parts of southeastern China because of substantial rainfalls as well as a large atmospheric demand (Figure 7b). It also appears that, for a given area, ET_a in the spring is overall higher than in autumn. This is especially true for eastern and central China, where spring ET_a mainly ranges between 170 and 230 mm (Figure 7a), while autumn ET_a drops to roughly 100–140 mm (Figure 7c). The spatial heterogeneity of ET_a becomes much less apparent in winter when ET_a is lower than 30 mm in most part of the country except for the southeastern coastal regions, southern Yunnan, and the southeastern Tibetan Plateau. Averaged over the whole country, the multiyear (1982–2012) mean seasonal ET_a is 225 ± 9 mm for summer, followed by 101 ± 7 mm for spring, 67 ± 4 mm for autumn, and 13 ± 1 mm for winter.

Figure 8 further displays the 31-year mean monthly CR-derived ET_a rates over China and its 10 major river basins. As seen, the annual amplitude of ET_a is overall higher in the humid regions (e.g., the Pearl River and Southeast River Basins) than in dry ones (e.g., the Northwest River Basin), which is consistent with the seasonal pattern of solar radiation and precipitation in China. The maximum monthly ET_a occurs in July for all basins, reaching more than 120 mm over four basins located in the southern China but dropping to approximately 90 mm over basins in the northern territories. The lowest July ET_a, as expected, is found in the driest Northwest River Basin with a value of only 47 mm. When considering the whole country, the maximum monthly ET_a rate also occurs in July with a value of 83 mm (Figure 8k).

3.4. Temporal Variations of ET_a

3.4.1. Annual ET_a

Spatially, the trends of annual ET_a during 1982–2012 are very heterogeneous in China (Figure 9a). Annual ET_a is found to increase significantly over most parts of western and northeastern China with rates of about 1–4 mm/year (e.g., Heilongjiang, western Inner Mongolia, and most parts of the Tibetan Plateau and Xinjiang). In the middle reaches of the Yangtze and Yellow River Basins, ET_a also increased to some extent but at a lower rate. Conversely, annual ET_a decreased significantly over most parts of the North China Plain and in the eastern and southern coastal regions with rates of −3 to −6 mm/year. In total, 14.1% and 26.3% of

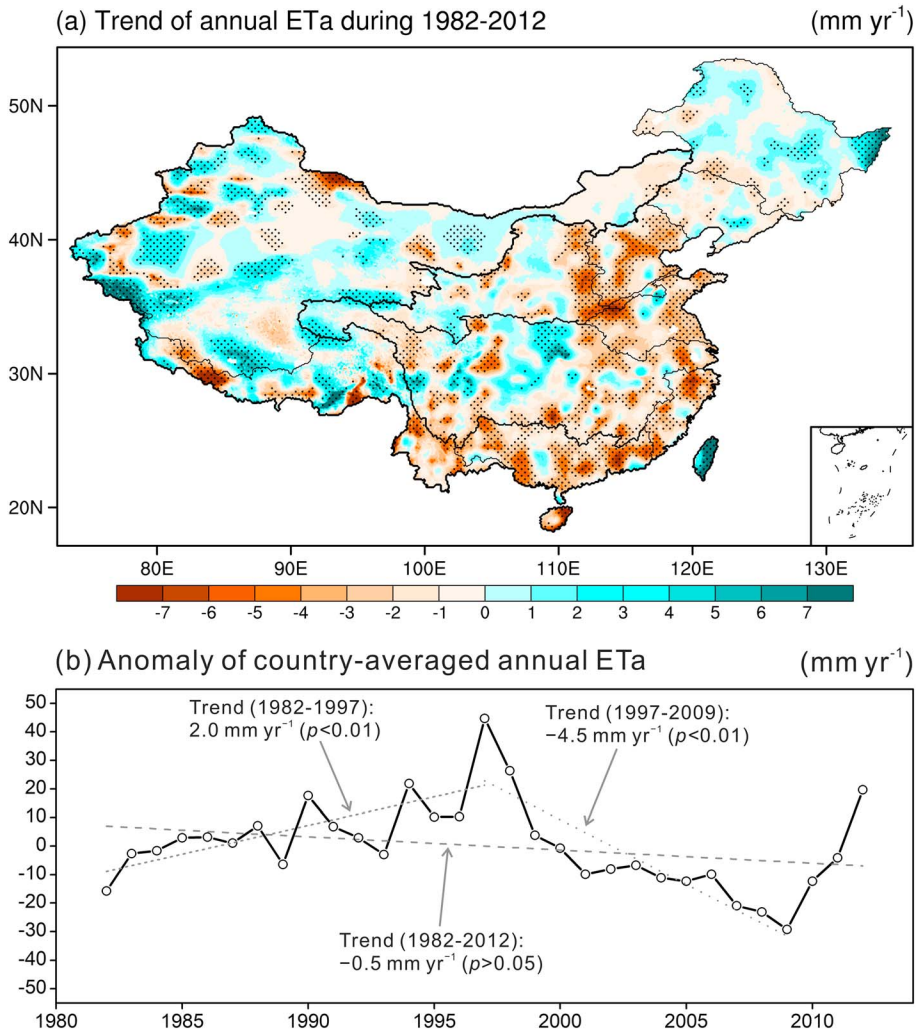

Figure 9. (a) Spatial pattern of complementary relationship-modeled annual ET_a trends during 1982–2012 across China. The stippling indicates trends that are statistically significant ($p < 0.05$); (b) anomaly of the country-averaged annual ET_a values with linear trends marked for three different periods.

the grid cells in China displayed significant increasing and decreasing trends for annual ET_a during 1982–2012, respectively; while the remaining 59.6% showed no significant trend during the same period.

Averaged over the whole country, annual ET_a displays a statistically insignificant decreasing trend during 1982–2012 with a rate of −0.5 mm/year ($p > 0.05$; Figure 9b). Annual ET_a displayed contrasting tendencies between pre-late and post-late 1990s. Specifically, annual ET_a increased significantly during 1982–1997 with a rate of 2.0 mm/year ($p < 0.01$), while a significant decline with a rate of −4.5 mm/year ($p < 0.01$) is observable during 1997–2009, though it increased rapidly in the subsequent 3 years. In short, the national-mean annual ET_a increased gradually from the early 1980s to the late 1990s, followed by a rapid decrease until the late 2000s.

3.4.2. Seasonal ET_a

The trends of seasonal ET_a during 1982–2012 also show a noticeable spatial heterogeneity across the country (Figure 10). Basically, the spatial pattern of the trends of summer ET_a is very similar to that of annual ET_a. Significant summer increases are found in western Inner Mongolia, the Tibetan Plateau, and northeastern China; while significant decreases in summer ET_a mainly occurred in the North China Plain, as well as in eastern and southern China (Figure 10b). Such a spatial pattern is also true overall for the trends of autumn ET_a but with lower magnitudes. In spring, however, ET_a increased over most parts of the country except for Yunnan, western Tibet, and parts of the Hai and Huai River basins, where ET_a showed significant decreasing trends over the past 31 years (Figure 10a). The trends in winter ET_a appear much more subdued than those

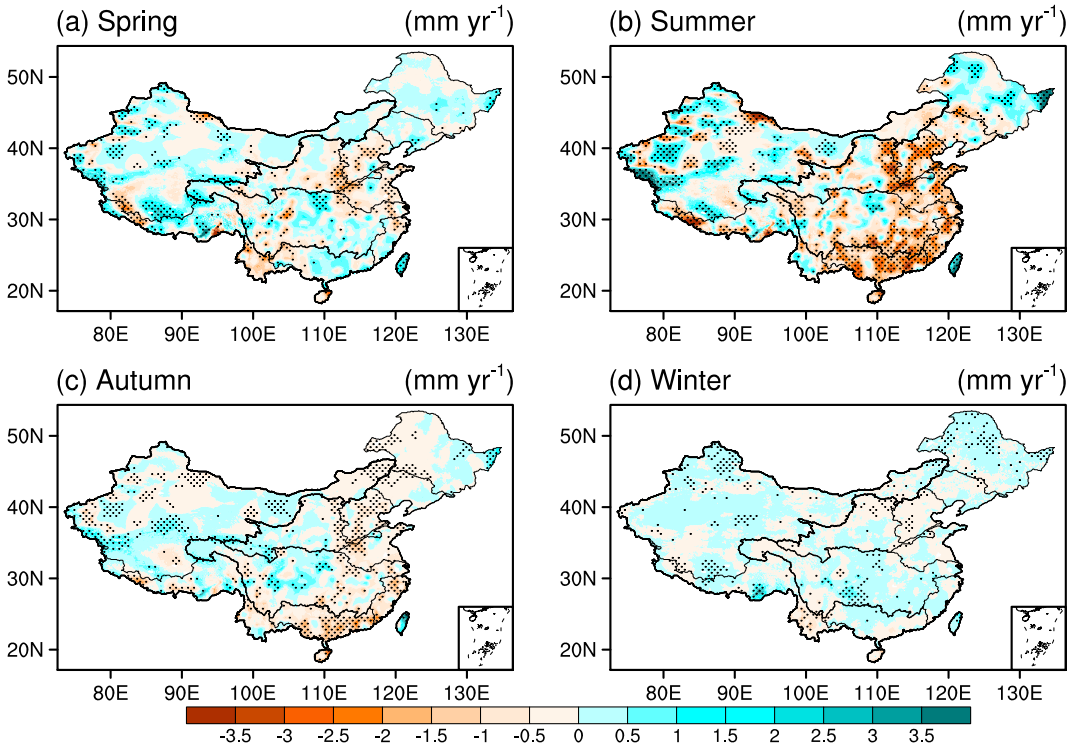

Figure 10. Complementary relationship-modeled seasonal ET_a trends (1982–2012) across China. The stippling indicates trends that are statistically significant ($p < 0.05$); (a) spring, (b) summer, (c) autumn, and (d) winter.

in other seasons, though ET_a during this season increased over most parts of Xinjiang, northeastern and southern China. In terms of the country-wide average seasonal ET_a values during 1982–2012 (figure not shown), however, there is no significant trend for the seasons except for summer which displayed a significant decline of −0.3 mm/year ($p < 0.05$).

4. Discussions

4.1. Uncertainties in the Model Validations

Although the present CR-simulated ET_a values are both validated by plot-scale EC observations and by basin-wide water-balance values, the uncertainties in these ground-truth data should be acknowledged. First, the EC-measured turbulent fluxes often suffer from a well-known energy closure problem (Foken, 2008; Stoy et al., 2013; Wilson et al., 2002) which could not be corrected in the present study because of the lack of available R_n and G data for most sites. It was reported that the residual of the energy balance closure typically ranges between 10% and 30% at most flux observation sites (Foken, 2008; Wilson et al., 2002), indicating a possible underestimation of the sensible and/or latent heat fluxes. Note also that additional uncertainties may be introduced when EC-measured ET_a results are compared to the modeled values of the 0.1° pixels, since the flux footprint of EC is primarily in the order of 1,000 m or less. Although we are aware of the mismatch between the source area of flux towers and the modeling grid, it is difficult to avoid such an uncertainty since long-term forcing data with a better spatial resolution than CMFD is yet unavailable in China (He & Yang, 2011). In this regard, more high-density ground EC observations at scales relevant to the modeling grid would benefit a thorough validation.

Second, the accuracy of the basin-scale water-balance-based evapotranspiration, ET_{wb}, values also relies on the validity of several assumptions. While one can assume that the subsurface leakage to adjacent basins is negligible for such large river basins, the human water extraction and/or reservoir regulations in highly populated areas of eastern and southern China may be substantial (Mao et al., 2016). This is especially true for the Hai River Basin where groundwater storage has been found to decrease significantly in recent years (Feng et al., 2018). Incorporation of the GRACE-observed ΔS in equation (11), however, accounts for such effects.

It should be noted that while runoff data are generally considered reliable, the uncertainty in the basin-scale precipitation values may also impact ET_{wb} to varying extent (Miralles et al., 2016), especially in less populated remote regions of highly varying topography since P is primarily interpolated from the point measurements of rain gauges. This is particularly the case for the Southwest River Basin which includes the southern and eastern parts of Tibetan Plateau, precipitation stations in this basin are mostly situated in valleys and few are higher than 3,000 m above sea level (Wang et al., 2018). Because of the orographic enhancement, precipitation estimation in such a way may be inaccurate. For example, Immerzeel et al. (2015), using an inverse estimation with glacier mass balance in high altitudes, found that the true precipitation rates in the western part of Tibetan Plateau should be more than twice as those from station-based interpolation and current precipitation products, indicating a remarkable underestimation in high-elevation precipitation. Consequently, the basin-scale precipitation of the Southwest River basin must be underestimated due to neglecting high-elevation precipitation, leading to an underestimation of ET_{wb} for such a basin by equation (11).

4.2. Sensitivity of the CR-Simulated ET_a Values to Model Forcing

Because the accuracy of the modeled ET_a depends to a large extent on the quality of gridded forcing (Badgley et al., 2015), it is worthwhile to address how possible biases in forcing impact the modeling results, even though CMFD is considered by far the highest quality climate data over China (Chen et al., 2011; He & Yang, 2011). Based on Zhou et al. (2015), the possible bias of downward shortwave radiation data in CMFD is on the order of 10%. We therefore assume an uncertainty of 10% for model forcing except for temperature where a half- and a one-degree change is introduced, similar to climate-change scenarios. In the sensitivity experiments, the CR model was rerun for 16 times by changing one forcing at a time while keeping other ones unperturbed. These included four groups of experiments, that is, (i) R_n and (ii) U_2 are perturbed by ±5% and ±10%, respectively; and (iii) T_a and (iv) T_d are changed by ±0.5 and ±1 °C, respectively.

It can be seen (Figure 11) that the CR model is most sensitive to R_n, as a 10% change of net radiation could cause ET_a vary by 12–15% over the 10 major river basins. The model, however, is the least sensitive to wind speed because a change of −10% in U_2 only leads to less than 2% change in ET_a. There were no remarkable sensitivity differences between T_a and T_d in the current CR model, except for their opposite effects. A potential positive bias of 1 °C in T_a would cause roughly −3 to −7% decreases in ET_a, while the same in T_d leads to 4–9% changes in ET_a over the river basins. Note also that sensitivity to a given forcing appears to be higher in dry basins than in humid ones (compare the slopes for the Northwest River basin with those of the Pearl and Southeast River Basins in each panel of Figure 11).

4.3. The Effect of Temporal Resolution in Forcing Data on the Model Results

The CR method has been widely used to estimate ET_a at annual (Hobbins et al., 2004), monthly (Liu et al., 2006; Szilagyi & Jozsa, 2008; Szilagyi, 2018a; Xu & Singh, 2005), weekly (Crago & Qualls, 2018), daily (Ma, Zhang, Szilagyi, et al., 2015; Ma, Zhang, Xu, et al., 2015; Ozdogan & Salvucci, 2004), and subdaily (Crago & Crowley, 2005; Han, Tian, et al., 2014) scales. However, Morton (1983) suggested to avoid using the CR for periods shorter than 5 days over extended periods of time and/or over a large regional scale since large-scale weather fronts may bring air masses over the land with a moisture signature decoupled from the underlying surface, which thus may temporarily disrupt the dynamic equilibrium of air humidity and surface fluxes in the land-atmosphere system. Consequently, the CR model was driven in the present study over China by forcing at a monthly time step during 1982–2012. While there is much nonlinearity of the processes in the coupled land-atmosphere system, this does not mean that such modeled ET_a rates would differ significantly from those driven by higher temporal resolution forcing (e.g., daily or hourly). To illustrate the point, additional CR modeling with forcing data ($R_n - G$, T_a, T_d, and U_2) observed at Miyun Station (Liu et al., 2013) during 2008–2010 at varying temporal resolutions was implemented (see Appendix C for details). The simulated results with finer temporal resolution (i.e., daily, 5-day mean, and 10-day mean) forcing were compared to the result driven by 30-day mean forcing (Figure S4). The CR model produced almost the same results for the 30-day aggregation of the ET_a values independent of what temporal resolution/averaging the forcing was applied. The RMSE between ET_a with daily forcing and that with 30-day mean forcing is only 1.7 mm per 30 days, thus suggesting that the present CR model is quite insensitive to the temporal resolution/aggregation of the model forcing.

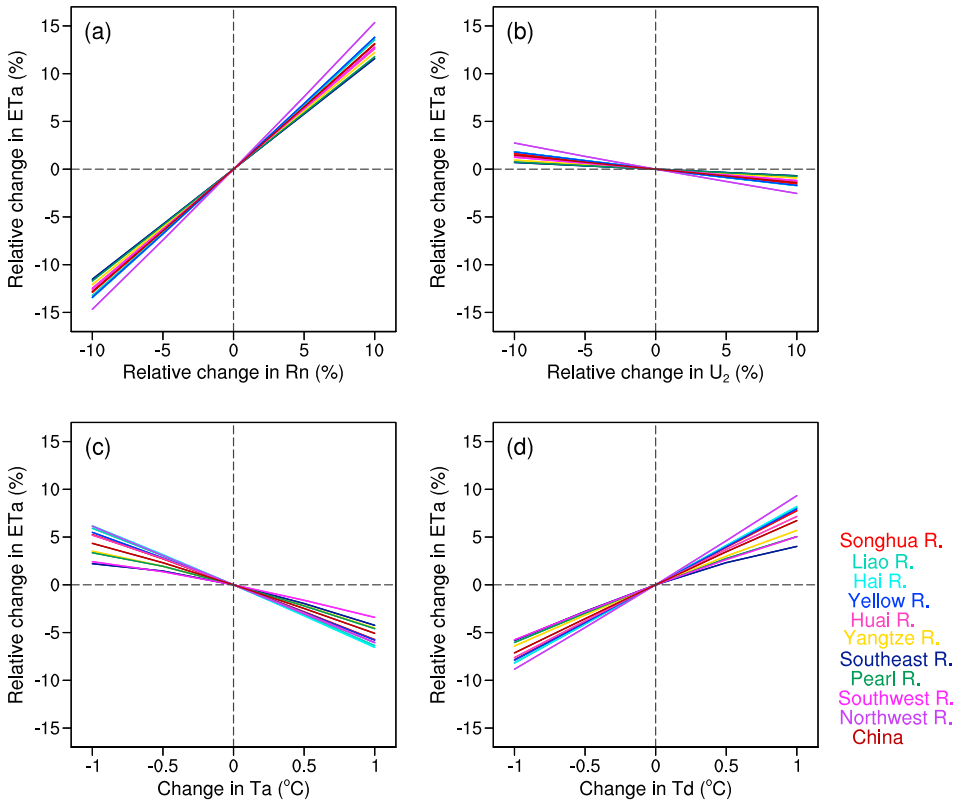

Figure 11. Sensitivity of the complementary relationship-modeled ET_a values to changes in (a) net radiation (R_n); (b) 2-m wind speed (U_2); (c) air temperature (T_a); and (d) dew-point temperature (T_d). Perturbations in R_n and U_2 are relative changes by −10%, −5%, 5% and 10%; while perturbations in T_a and T_d are absolute changes by −1, −0.5, 0.5 and 1 °C. Mean annual (1982–2012) ET_a values of the perturbed forcing are scaled by the simulation results of the unperturbed forcing for each river basin and the whole country.

4.4. Magnitudes and Trends in Annual ET_a Over China

Similar to previous findings of substantial differences in ET_a among reanalysis, LSM, and RS methods at a global scale (Mueller et al., 2013), a large discrepancy in ET_a estimates for China has also been reported among different ET_a products, yielding a wide range of 350–700 mm/year for the country-averaged multi-year mean ET_a (Chen et al., 2014; Li, Liang, et al., 2014; Mao & Wang, 2017; Su et al., 2015; Sun et al., 2017; Yang et al., 2018). In view of the long-term, country-wide average precipitation rate of about 720 mm/year (based on the records of roughly 2,400 rain gauges from 1956 to 2013 by Ren et al., 2015) and runoff of about 280 mm/year (from the Variable Infiltration Capacity model for the 1956–2005 period by Wang et al., 2012) for China, however, we argue that any value higher than 440 mm/year for the country-representative climatological mean annual ET_a may be considered unrealistic. In this context, the country-averaged multiyear mean annual ET_a rate of 406 mm/year from the CR model should be reasonable for China. Previous model intercomparisons by Miralles et al. (2016) and Mueller et al. (2013) have found that reanalysis-based ET_a is much higher than those from LSM- and RS-based products. Hence, it is believed that the multiyear mean values of 511 mm/year from ERA-Interim and 506 mm/year from JRA-55 (Figure 6) are also inflated values for China. A recent validation study by Bai and Liu (2018) concluded that three ET_a products (i.e., GLEAM, CLSM, and another product from the Numerical Terradynamic Simulation Group) remarkably overestimate ET_a in comparison with water balance-based results in the Chinese humid basins, thus indicating the values of GLEAM and CLSM in Figure 6 may also overestimate ET_a of China to some extent.

The increase in CR-modeled ET_a for most parts of western and northeastern China and the decrease for most parts of southern and eastern China are overall consistent with the results of a long-term water-balance analysis by Gao et al. (2007), who concluded that ET_a had a decreasing trend in most areas east of 100°E but

showed an increasing trend in the western and the northern parts of northeastern China. Furthermore, Han, Tian, et al. (2014) also identified obvious decreasing trends in annual ET_a over the past few decades for most stations in the humid regions while found the opposite for most stations in the arid regions. The decrease of ET_a over the last three decades reported in the present study for the North China Plain is supported by the significant decline in topsoil water content during 1983–2012, which was due partially to the intensification of agricultural activities, as was demonstrated by Liu et al. (2015). In terms of the variations of country-averaged annual ET_a over last three decades, we found contrasting trends between pre-late and post-late 1990s. This is consistent with the conclusion of Mao and Wang (2017), which employed a modified Penman-Monteith model driven by forcing of 2,479 weather stations across China.

4.5. From Calibrated to Calibration-Free CR Modeling of Large-Scale ET_a

The exceptional feature of the present CR method for long-term and large-scale ET_a estimation is that it requires only routine meteorological data (Brutsaert, 2015; Crago & Qualls, 2013). However, most existing CR-based models are developed and/or calibrated by prior knowledge of ET_a (either by water-balance-derived or EC-measured; e.g., Brutsaert, 2015; Brutsaert & Stricker, 1979; Granger, 1989; Han et al., 2012), as was done by, for example, Hobbins et al. (2001) in the continental United States, C. Xu and Singh (2005) in three basins with different climates, Liu, Liu, et al. (2016) in the eastern monsoon region of China, and by a variety of site-specific ET_a simulations (Brutsaert et al., 2017; Crago & Qualls, 2018; Han, Xu, et al., 2014; Ma, Zhang, Xu, et al., 2015). As such, the CR model may become computationally expensive. Additionally, regarding Brutsaert's (2015) nonlinear CR model, the calibrated α appears to vary significantly with different ecosystems (Brutsaert et al., 2017; Hu et al., 2018; Liu, Liu, et al., 2016; Zhang et al., 2017) and its controlling factors remain controversial (see different conclusions in Liu, Liu, et al., 2016, and Hu et al., 2018), constraining the agility of this model in large-scale ET_a simulation covering different terrestrial ecosystems.

In the present study, a more general approach that adopts an inversion of the Priestley-Taylor equation is employed to obtain an appropriate α value for China (see Appendix A for how it was derived). It involves the identification of wet grid cells (Szilagyi et al., 2017) without resorting to measured precipitation, runoff, or ET_a data and by doing so avoids the typically time-consuming classical calibration process (e.g., the trial-and-error method). Note that such model calibrations in general may be hindered by (i) a lack of measured/water-balance-based ET_a data and/or (ii) limited spatial representativeness and relevance of available ET_a. In short, the most important advantage of the present Szilagyi et al. (2017) CR model is (a) the avoidance of parameter optimization to local conditions, which to a large extent improves the computational efficiency, and (b) it also circumvents the difficulty of finding ground-truth ET_a data for model calibration.

It should be noted that the value of the α parameter is never intended to be a constant (Brutsaert, 2015). With its vast territory, China features climate conditions that vary greatly among the different regions. In this way, a mean value from wet grids does not mean it is optimal anywhere in China due to the intricate effect of topography, land cover conditions, and the resulting atmospheric boundary layer. This partially explains why the simulated ET_a by the present CR method still displays biases in certain river basins (see Figure 3). Additional basin-specific calibration of the model parameter α and also more accurate meteorological forcing may further facilitate an improved ET_a modeling in the future.

5. Conclusions

ET_a over China during 1982–2012 was simulated by a calibration-free nonlinear CR model (Szilagyi et al., 2017) with inputs of air and dew-point temperature, wind speed, and net radiation. Multiscale validations employing EC-measured and water-balance-derived evapotranspiration data suggest that the CR-simulated ET_a rates are reliable, even though the key parameter of the model, the Priestley-Taylor coefficient, was not calibrated against any prior ground-truth ET_a data. The present CR-based ET_a product is an improvement over existing similar products in its (i) higher spatial resolution of 0.1°; (ii) minimal data requirement; and (iii) improved model accuracy, as was demonstrated with the help of eight mainstream ET_a products, where the CR model excelled seven of them. In general, this CR-based method may become useful in continental-to-global-scale hydrological research as it can help future calibrations/verifications of the complex LSM- and RS-based models, which need extensive soil and vegetation data as inputs. Further, it may also serve as a potential benchmarking tool due to its calibration-free nature and minimal data requirement.

The multiyear, country-wide mean annual ET_a over China is 406 ± 15 mm/year by the present CR-based model. The maximum is found in Hainan province (>1,200 mm/year) and the minimum in the Taklamakan Desert (<50 mm/year). Annual ET_a generally decreases from the southeast to the northwest following the pattern of the annual aridity index over China. Averaged over the whole country, annual ET_a increased significantly during 1982–1997, while the reverse was seen after 1997. Overall, there was a slight decrease in country-averaged annual ET_a with a rate of −0.5 mm/year ($p = 0.86$) in China during 1982–2012. However, the trends in annual ET_a are spatially heterogeneous in China, with 14% and 26% grid cells expressing significantly increasing and decreasing trends during 1982–2012, respectively; while the remaining 60% showing no obvious long-term tendencies. In general, a rising trend of annual ET_a dominates in the western and northeastern parts of China over the past three decades, while the opposite is primarily found in the North China Plain and in most parts of eastern and southern China.

Appendix A: Setting the Value of α for China

The Bowen ratio of a wet-environment can be obtained with the help of the Priestley and Taylor (1972) equation (6), as

$$\frac{1-\alpha\frac{\Delta_{Twea}}{\Delta_{Twea}+\gamma}}{\alpha\frac{\Delta_{Twea}}{\Delta_{Twea}+\gamma}}=\gamma\frac{T_{wes}-T_a}{e_{o,Twes}-e_a}, \tag{A1}$$

in which all variables are defined in section 2.1. The left side of equation (A1) is the Bowen ratio by employing equation (6), while the right side is written as the temperature and humidity gradients above the wet surface (Bowen, 1926). After rearrangement of (A1), one obtains

$$\alpha=\frac{(\Delta_{Twea}+\gamma)(e_{o,Twes}-e_a)}{\Delta_{Twea}\left[\gamma(T_{wes}-T_a)+(e_{o,Twes}-e_a)\right]}. \tag{A2}$$

For large-scale gridded data, it is possible to identify wet cells that satisfy certain predefined requirements, thereby calculating their α values within the theoretical limits of [1, (Δ_{Twea} + γ) / Δ_{Twea}] (Priestley & Taylor, 1972). Note that when a cell is wet, then T_{wea} in (A2) equals the measured T_a. Following Szilagyi et al. (2017), a grid cell is considered "wet" provided $T_{wes} > T_a + 2$ °C and relative humidity is larger than 90% in the present study. Relative humidity is derived using T_a, q, and *Pres* data from CMFD. T_{wes} comes from equation (7) and here should not be limited by T_a over wet cells. The average value of α coming from such wet cells yielded a value of 1.12 for China, which was retained for use in the current CR model.

Appendix B: Deriving R_n for 1982–2012 Across China

The net radiation (R_n) was derived from net shortwave radiation and longwave radiation as

$$R_n=(1-ALB)\times DSR+\varepsilon DLR-\varepsilon\sigma LST^4, \tag{B1}$$

where *DSR* (W/m^2) and *DLR* (W/m^2) are the downward shortwave and longwave radiation, respectively, which are available in CMFD at a spatial resolution of 0.1°. The ε is the surface thermal broadband emissivity, σ the Stefan-Boltzmann constant (5.67×10^{-8} W·m^{-2}·K^{-4}), and *LST* the land surface temperature (K). The last term in equation (B1) is the upward longwave radiation. The *ALB*, also called blue-sky albedo, is the ratio of the reflected to incident solar radiation. Note that most, if not all, current albedo products only provide the black-sky albedo (*BSA*, i.e., directional hemispherical reflectance) and/or the white-sky albedo (*WSA*, i.e., bihemispherical reflectance; see Table 1 in He et al., 2014), both of which are not equal to *ALB*, though the difference between them may not be large (Román et al., 2010). To be more precise, the *ALB* could be derived by (He et al., 2014; Román et al., 2010):

$$ALB=\left(1-f_{dif}\right)\times BSA+f_{dif}\times WSA, \tag{B2}$$

where f_{dif} is the diffuse skylight ratio. The 8-day 0.05° *BSA* and *WSA* during 1982–2012 from the GLASS albedo product (Liang et al., 2013), which is produced from the Advanced Very High Resolution

Radiometer (1982–1999) and MODIS (2000–2012) data, were used in equation (B2). They were aggregated to monthly mean values. The monthly diffuse and direct downward radiation data for 1982–2012 from the National Centers for Environmental Prediction reanalysis (Kalnay et al., 1996) were used to calculate f_{dif}, that is,

$$f_{dif} = (DD_v + DD_{nir})/(DD_v + DD_{nir} + BD_v + BD_{nir}), \quad \text{(B3)}$$

in which DD_v and DD_{nir} are the diffuse downward solar flux in the visible band and in the near-infrared band, respectively. BD_v and BD_{nir} are the direct downward solar flux in the visible band and in the near-infrared band, respectively. The (B3)-computed f_{dif} values were resampled to 0.05° to fit the spatial resolution of the GLASS albedo product.

The GLASS longwave broadband emissivity data at a resolution of 0.05° for 1982–2012 (Liang et al., 2013; Cheng et al., 2016), which is produced by using Advanced Very High Resolution Radiometer visible and near-infrared reflectance (1982–1999) and MODIS seven black-sky albedos (2000–2012), were employed for ε in equation (B1), Finally, both 0.05° *ALB* and ε values were aggregated to 0.1°.

LST data came from the monthly MODIS Terra (MOD11C3) and Aqua (MYD11C3) LST products at a spatial resolution of 0.05° (Wan, 2014). It should be noted that both MOD11C3 and MYD11C3 provide two instantaneous *LST* records per day including a daytime and a nighttime observation, that is, Terra night (LST_{TN}), Terra day (LST_{TD}), Aqua night (LST_{AN}), and Aqua day (LST_{AD}), which are observed at local times of roughly 22:30, 10:30, 1:30, and 13:30, respectively (Zhang et al., 2018). Note also that the Terra satellite started its observations on 24 February 2000, while the Aqua satellite was initiated on 4 July 2002. This way, the monthly *LST* during July 2002 to December 2012 was calculated as the arithmetic mean of monthly LST_{TN}, LST_{TD}, LST_{AN}, and LST_{AD}. During February 2000 to June 2002, only the first two (i.e., LST_{TN} and LST_{TD}) were averaged to calculate the monthly *LST*. The derived monthly *LST* during February 2000 to December 2002 were subsequently resampled to 0.1° to fit the spatial resolution of the CMFD data set. As for the *LST* prior to January 2000, the multiyear mean monthly differences between *LST* and T_a (i.e., $LST - T_a$) for 2000–2012 were first calculated. By assuming invariant monthly ($LST - T_a$) differences for each month, the monthly *LST* during January 1982 to January 2000 were then reconstructed using T_a of CMFD from the same period.

Appendix C: Modeling Experiment With Different Temporal Resolutions of Forcing

At Miyun station (Liu et al., 2013), the net radiation, soil heat flux, air temperate, relative humidity, air pressure, and wind speed were measured over an orchard from January 2008 to December 2010 (Table 1, available online http://westdc.westgis.ac.cn/data/486fe849-81ca-454f-955d-c3152715a956; Liu & Xu, 2013). The raw 10-min observed data were first aggregated into daily values. Days during which (i) any 10-min gaps occurred, or (ii) daily available energy was negative were excluded. The remaining 923 days of daily data were renumbered from 1 to 923 according to the original ordinal day. For the creation of complete 30-day groups of data, only the first 900 days were used (i.e., 30 groups with 30-day worth of data in each). Four scenarios of forcing with different time resolutions, that is, daily, 5-, 10-, and 30-day averaged were constructed for each group, which were then used to drive the CR model (equation (1)) with an identical α value of 1.12. The modeled ET_a rates in each group were then summed up to become 30-day ET_a values. These 30-day ET_a values driven by different resolution forcing were subsequently compared (Figure S4). Note that this way, the 30-day ET_a rates are not exactly the same as the monthly ET_a rates in Figure 2 since (i) days with data gaps or negative available energy are removed, and (ii) CMFD forcing, to some extent, presumably differ from the in situ observed meteorological data of Miyun Station.

Acknowledgments
This research was jointly funded by the Strategic Priority Research Program (A) of CAS (XDA2006020102), National Key Research and Development Program of China (2017YFA0603101), National Natural Science Foundation of China (41430748, 41801047, and 41661144025), CAS International Cooperation Program (131C11KYSB20160061), BME-Water Sciences & Disaster Prevention FIKP grant of EMMI (BME FIKP-VIZ), and China Postdoctoral Science Foundation (2017LH032). The manuscript benefited greatly from the comments by Adriaan Teuling and another two anonymous reviewers. We appreciate the Principal Investigators of EC stations listed in Table 1 for sharing their observed data. We especially thank Shaomin Liu (Beijing Normal University) for sharing the Miyun station data and Zengchuan Dong (Hohai University) for his guidance in the Water Resource Bulletin data. All data used in this study can be freely accessed from the cited websites described in the text, and we thank all organizations and persons for making such data available to the public. The estimated R_n data are available from the corresponding author. The CR-based ET_a product will be archived in the TPE database (http://en.tpedatabase.cn/).

References

Allen, R. G., Pereira, L. S., Raes, D., & Smith, M. (1998). *Crop evapotranspiration—Guidelines for computing crop water requirements*. Rome, Italy: Food and Agriculture Organization.

Badgley, G., Fisher, J. B., Jiménez, C., Tu, K. P., & Vinukollu, R. (2015). On uncertainty in global terrestrial evapotranspiration estimates from choice of input forcing datasets. *Journal of Hydrometeorology*, *16*(4), 1449–1455. https://doi.org/10.1175/JHM-D-14-0040.1

Bai, P., & Liu, X. (2018). Intercomparison and evaluation of three global high-resolution evapotranspiration products across China. *Journal of Hydrology*, *566*, 743–755. https://doi.org/10.1016/j.jhydrol.2018.09.065

Baik, J., Liaqat, U. W., & Choi, M. (2018). Assessment of satellite- and reanalysis-based evapotranspiration products with two blending approaches over the complex landscapes and climates of Australia. *Agricultural and Forest Meteorology*, *263*, 388–398. https://doi.org/10.1016/j.agrformet.2018.09.007

Baldocchi, D. D., Falge, E., Gu, L., Olson, R., Hollinger, D., Running, S., et al. (2001). FLUXNET: A new tool to study the temporal and spatial variability of ecosystem-scale carbon dioxide, water vapor, and energy flux densities. *Bulletin of the American Meteorological Society*, *82*(11), 2415–2434. https://doi.org/10.1175/1520-0477(2001)082<2415:FANTTS>2.3.CO;2

Beaudoing, H., & Rodell, M. (2015). GLDAS Noah Land Surface Model L4 3 hourly 0.25 x 0.25 degree V2.0, Greenbelt, Maryland, USA. Goddard Earth Sciences Data and Information Services Center (GES DISC). doi: https://doi.org/10.5067/342OHQM9AK6Q

Bonan, G. B., Levis, S., Kergoat, L., & Oleson, K. W. (2002). Landscapes as patches of plant functional types: An integrating concept for climate and ecosystem models. *Global Biogeochemical Cycles*, *16*(2), 1021. https://doi.org/10.1029/2000GB001360

Bouchet, R. J. (1963). Evapotranspiration réelle et potentielle, signification climatique. *International Association of Scientific Hydrology. Publication*, *62*, 134–142.

Bowen, I. S. (1926). The ratio of heat losses by conduction and by evaporation from any water surface. *Physical Review*, *27*(6), 779–787. https://doi.org/10.1103/PhysRev.27.779

Brutsaert, W. (2005). *Hydrology: An introduction*. New York: Cambridge University Press. https://doi.org/10.1017/CBO9780511808470

Brutsaert, W. (2015). A generalized complementary principle with physical constraints for land-surface evaporation. *Water Resources Research*, *51*, 8087–8093. https://doi.org/10.1002/2015WR017720

Brutsaert, W., Li, W., Takahashi, A., Hiyama, T., Zhang, L., & Liu, W. (2017). Nonlinear advection-aridity method for landscape evaporation and its application during the growing season in the southern Loess Plateau of the Yellow River Basin. *Water Resources Research*, *53*, 270–282. https://doi.org/10.1002/2016WR019472

Brutsaert, W., & Stricker, H. (1979). An advection-aridity approach to estimate actual regional evapotranspiration. *Water Resources Research*, *15*(2), 443–450. https://doi.org/10.1029/WR015i002p00443

Chen, F., & Dudhia, J. (2001). Coupling an advanced land surface-hydrology model with the Penn State-NCAR MM5 modeling system. Part I: Model implementation and sensitivity. *Monthly Weather Review*, *129*(4), 569–585. https://doi.org/10.1175/1520-0493(2001)129<0569:CAALSH>2.0.CO;2

Chen, F., & Zhang, Y. (2009). On the coupling strength between the land surface and the atmosphere: From viewpoint of surface exchange coefficients. *Geophysical Research Letters*, *36*, L10404. https://doi.org/10.1029/2009GL037980

Chen, S., Chen, J., Lin, G., Zhang, W., Miao, H., Wei, L., et al. (2009). Energy balance and partition in Inner Mongolia steppe ecosystems with different land use types. *Agricultural and Forest Meteorology*, *149*(11), 1800–1809. https://doi.org/10.1016/j.agrformet.2009.06.009

Chen, Y., Xia, J., Liang, S., Feng, J., Fisher, J. B., Li, X., et al. (2014). Comparison of satellite-based evapotranspiration models over terrestrial ecosystems in China. *Remote Sensing of Environment*, *140*, 279–293. https://doi.org/10.1016/j.rse.2013.08.045

Chen, Y., Yang, K., He, J., Qin, J., Shi, J., Du, J., & He, Q. (2011). Improving land surface temperature modeling for dry land of China. *Journal of Geophysical Research*, *116*, D20104. https://doi.org/10.1029/2011JD015921

Cheng, J., Liang, S., Verhoef, W., Shi, L., & Liu, Q. (2016). Estimating the hemispherical broadband longwave emissivity of global vegetated surfaces using a radiative transfer model. *IEEE Transactions on Geoscience and Remote Sensing*, *54*(2), 905–917. https://doi.org/10.1109/tgrs.2015.2469535

Chu, H., Baldocchi, D. D., John, R., Wolf, S., & Reichstein, M. (2017). Fluxes all of the time? A primer on the temporal representativeness of FLUXNET. *Journal of Geophysical Research: Biogeosciences*, *122*, 289–307. https://doi.org/10.1002/2016JG003576

Chu, Q., Xu, Z., Peng, D., Yang, X., & Yang, G. (2015). Trends of surface humidity and temperature during 1951—2012 in Beijing, China. *Proceedings of the International Association of Hydrological Sciences*, *368*, 126–131. https://doi.org/10.5194/piahs-368-126-2015

Clark, M. P., Fan, Y., Lawrence, D. M., Adam, J. C., Bolster, D., Gochis, D. J., et al. (2015). Improving the representation of hydrologic processes in earth system models. *Water Resources Research*, *51*, 5929–5956. https://doi.org/10.1002/2015WR017096

Crago, R., & Crowley, R. (2005). Complementary relationships for near-instantaneous evaporation. *Journal of Hydrology*, *300*(1–4), 199–211 . https://doi.org/10.1016/j.jhydrol.2004.06.002

Crago, R., & Qualls, R. (2013). The value of intuitive concepts in evaporation research. *Water Resources Research*, *49*, 6100–6104. https://doi.org/10.1002/wrcr.20420

Crago, R., Szilagyi, J., Qualls, R. J., & Huntington, J. (2016). Rescaling of the complementary relationship for land surface evaporation. *Water Resources Research*, *52*, 8461–8471. https://doi.org/10.1002/2016WR019753

Crago, R. D., & Qualls, R. J. (2018). Evaluation of the generalized and rescaled complementary evaporation relationships. *Water Resources Research*, *54*, 8086–8102. https://doi.org/10.1029/2018WR023401

Dee, D. P., Uppala, S. M., Simmons, A. J., Berrisford, P., Poli, P., Kobayashi, S., et al. (2011). The ERA-Interim reanalysis: Configuration and performance of the data assimilation system. *Quarterly Journal of the Royal Meteorological Society*, *137*(656), 553–597. https://doi.org/10.1002/qj.828

Dirmeyer, P. A., Gao, X., Zhao, M., Guo, Z., Oki, T., & Hanasaki, N. (2006). GSWP-2: Multimodel analysis and implications for our perception of the land surface. *Bulletin of the American Meteorological Society*, *87*(10), 1381–1398. https://doi.org/10.1175/bams-87-10-1381

Feng, W., Shum, C., Zhong, M., & Pan, Y. (2018). Groundwater storage changes in China from satellite gravity: An overview. *Remote Sensing*, *10*(5), 674. https://doi.org/10.3390/rs10050674

Fisher, J. B., Melton, F., Middleton, E., Hain, C., Anderson, M., Allen, R., et al. (2017). The future of evapotranspiration: Global requirements for ecosystem functioning, carbon and climate feedbacks, agricultural management, and water resources. *Water Resources Research*, *53*, 2618–2626. https://doi.org/10.1002/2016WR020175

Foken, T. (2008). The energy balance closure problem: An overview. *Ecological Applications*, *18*(6), 1351–1367. https://doi.org/10.1890/06-0922.1

Gao, G., Chen, D., Xu, C.-Y., & Simelton, E. (2007). Trend of estimated actual evapotranspiration over China during 1960–2002. *Journal of Geophysical Research*, *112*, D11120. https://doi.org/10.1029/2006JD008010

Granger, R. J. (1989). A complementary relationship approach for evaporation from nonsaturated surfaces. *Journal of Hydrology*, *111*(1-4), 31–38. https://doi.org/10.1016/0022-1694(89)90250-3

Han, E., Crow, W. T., Hain, C. R., & Anderson, M. C. (2015). On the use of a water balance to evaluate interannual terrestrial ET variability. *Journal of Hydrometeorology*, *16*(3), 1102–1108. https://doi.org/10.1175/jhm-d-14-0175.1

Han, S., Hu, H., & Tian, F. (2012). A nonlinear function approach for the normalized complementary relationship evaporation model. *Hydrological Processes*, *26*(26), 3973–3981. https://doi.org/10.1002/hyp.8414

Han, S., Tian, F., & Hu, H. (2014). Positive or negative correlation between actual and potential evaporation? Evaluating using a nonlinear complementary relationship model. *Water Resources Research*, *50*, 1322–1336. https://doi.org/10.1002/2013WR014151

Han, S., Xu, D., Wang, S., & Yang, Z. (2014). Similarities and differences of two evapotranspiration models with routinely measured meteorological variables: Application to a cropland and grassland in Northeast China. *Theoretical and Applied Climatology*, *117*(3-4), 501–510. https://doi.org/10.1007/s00704-013-1016-8

Hao, Y., Wang, Y., Huang, X., Cui, X., Zhou, X., Wang, S., et al. (2007). Seasonal and interannual variation in water vapor and energy exchange over a typical steppe in Inner Mongolia, China. *Agricultural and Forest Meteorology*, *146*(1-2), 57–69. https://doi.org/10.1016/j.agrformet.2007.05.005

He, J., & Yang, K. (2011). China meteorological forcing dataset. Cold and Arid Regions Science Data Center at Lanzhou. https://doi.org/10.3972/westdc.002.2014.db

He, T., Liang, S., & Song, D.-X. (2014). Analysis of global land surface albedo climatology and spatial-temporal variation during 1981–2010 from multiple satellite products. *Journal Geophysical Research: Atmospheres*, *119*, 10,281–10,298. https://doi.org/10.1002/2014JD021667

Hobbins, M. T., Ramírez, J. A., & Brown, T. C. (2001). The complementary relationship in estimation of regional evapotranspiration: An enhanced advection-aridity model. *Water Resources Research*, *37*(5), 1389–1403. https://doi.org/10.1029/2000WR900359

Hobbins, M. T., Ramírez, J. A., & Brown, T. C. (2004). Trends in pan evaporation and actual evapotranspiration across the conterminous U. S.: Paradoxical or complementary? *Geophysical Research Letters*, *31*, L13503. https://doi.org/10.1029/2004GL019846

Hu, Z., Wang, G., Sun, X., Zhu, W., Song, C., Huang, K., & Chen, X. (2018). Spatial-temporal patterns of evapotranspiration along an elevation gradient on Mount Gongga, Southwest China. *Water Resources Research*, *54*, 4180–4192. https://doi.org/10.1029/2018WR022645

Immerzeel, W. W., van Beek, L. P., & Bierkens, M. F. (2010). Climate change will affect the Asian water towers. *Science*, *328*(5984), 1382–1385. https://doi.org/10.1126/science.1183188

Immerzeel, W. W., Wanders, N., Lutz, A. F., Shea, J. M., & Bierkens, M. F. P. (2015). Reconciling high-altitude precipitation in the upper Indus basin with glacier mass balances and runoff. *Hydrology and Earth System Sciences*, *19*(11), 4673–4687. https://doi.org/10.5194/hess-19-4673-2015

Jiménez, C., Prigent, C., Mueller, B., Seneviratne, S. I., McCabe, M. F., Wood, E. F., et al. (2011). Global intercomparison of 12 land surface heat flux estimates. *Journal of Geophysical Research*, *116*, D02102. https://doi.org/10.1029/2010JD014545

Jung, M., Reichstein, M., Ciais, P., Seneviratne, S. I., Sheffield, J., Goulden, M. L., et al. (2010). Recent decline in the global land evapotranspiration trend due to limited moisture supply. *Nature*, *467*(7318), 951–954. https://doi.org/10.1038/nature09396

Jung, M., Reichstein, M., Margolis, H. A., Cescatti, A., Richardson, A. D., Arain, M. A., et al. (2011). Global patterns of land-atmosphere fluxes of carbon dioxide, latent heat, and sensible heat derived from eddy covariance, satellite, and meteorological observations. *Journal of Geophysical Research*, *116*, G00J07. https://doi.org/10.1029/2010JG001566

Kalnay, E., Kanamitsu, M., Kistler, R., Collins, W., Deaven, D., Gandin, L., et al. (1996). The NCEP/NCAR 40-year reanalysis project. *Bulletin of the American Meteorological Society*, *77*(3), 437–471. https://doi.org/10.1175/1520-0477(1996)077<0437:TNYRP>2.0.CO;2

Kato, T., Tang, Y., Gu, S., Hirota, M., Du, M., Li, Y., & Zhao, X. (2006). Temperature and biomass influences on interannual changes in CO2 exchange in an alpine meadow on the Qinghai-Tibetan Plateau. *Global Change Biology*, *12*(7), 1285–1298. https://doi.org/10.1111/j.1365-2486.2006.01153.x

Kobayashi, S., Ota, Y., Harada, Y., Ebita, A., Moriya, M., Onoda, H., et al. (2015). The JRA-55 reanalysis: General specifications and basic characteristics. *Journal of the Meteorological Society of Japan*, *93*(1), 5–48. https://doi.org/10.2151/jmsj.2015-001

Koster, R. D., Suarez, M. J., Ducharne, A., Stieglitz, M., & Kumar, P. (2000). A catchment-based approach to modeling land surface processes in a general circulation model: 1. Model structure. *Journal of Geophysical Research*, *105*(D20), 24809–24822. https://doi.org/10.1029/2000JD900327

Kustas, W. P., Daughtry, C. S. T., & Van Oevelen, P. J. (1993). Analytical treatment of the relationships between soil heat flux/net radiation ratio and vegetation indices. *Remote Sensing of Environment*, *46*(3), 319–330. https://doi.org/10.1016/0034-4257(93)90052-Y

Landerer, F. W., & Swenson, S. C. (2012). Accuracy of scaled GRACE terrestrial water storage estimates. *Water Resources Research*, *48*, W04531. https://doi.org/10.1029/2011WR011453

Lawrence, D. M., Oleson, K. W., Flanner, M. G., Thornton, P. E., Swenson, S. C., Lawrence, P. J., et al. (2011). Parameterization improvements and functional and structural advances in version 4 of the Community Land Model. *Journal of Advances in Modeling Earth Systems*, *3*, M03001. https://doi.org/10.1029/2011ms000045

Li, B., Beaudoing, H., & Rodell, M. (2018). GLDAS Catchment Land Surface Model L4 daily 0.25 x 0.25 degree V2.0, Greenbelt, Maryland, USA. Goddard Earth Sciences Data and Information Services Center (GES DISC). doi: 0.5067/LYHA9088MFWQ

Li, X., Li, X., Li, Z., Ma, M., Wang, J., Xiao, Q., et al. (2009). Watershed allied telemetry experimental research. *Journal of Geophysical Research*, *114*, D22103. https://doi.org/10.1029/2008JD011590

Li, X., Liang, S., Yuan, W., Yu, G., Cheng, X., Chen, Y., et al. (2014). Estimation of evapotranspiration over the terrestrial ecosystems in China. *Ecohydrology*, *7*(1), 139–149. https://doi.org/10.1002/eco.1341

Li, Y., Cao, J., Shen, F., & Xia, J. (2014). The changes of renewable water resources in China during 1956–2010. *Science China Earth Sciences*, *57*(8), 1825–1833. https://doi.org/10.1007/s11430-013-4818-8

Liang, S., Zhao, X., Liu, S., Yuan, W., Cheng, X., Xiao, Z., et al. (2013). A long-term Global LAnd Surface Satellite (GLASS) data-set for environmental studies. *International Journal of Digital Earth*, *6*(sup1), 5–33. https://doi.org/10.1080/17538947.2013.805262

Liu, R., Li, Y., & Wang, Q.-X. (2012). Variations in water and CO_2 fluxes over a saline desert in western China. *Hydrological Processes*, *26*(4), 513–522. https://doi.org/10.1002/hyp.8147

Liu, S., Sun, R., Sun, Z., Li, X., & Liu, C. (2006). Evaluation of three complementary relationship approaches for evapotranspiration over the Yellow River Basin. *Hydrological Processes*, *20*(11), 2347–2361. https://doi.org/10.1002/hyp.6048

Liu S., & Xu Z. (2013) Multi-scale surface flux and meteorological elements observation dataset in the Hai River Basin (Miyun site-automatic weather station), Cold and Arid Regions Science Data Center at Lanzhou, doi: https://doi.org/10.3972/haihe.001.2013.db

Liu, S., Xu, Z. W., Zhu, Z. L., Jia, Z. Z., & Zhu, M. J. (2013). Measurements of evapotranspiration from eddy-covariance systems and large aperture scintillometers in the Hai River Basin, China. *Journal of Hydrology*, *487*, 24–38. https://doi.org/10.1016/j.jhydrol.2013.02.025

Liu, W., Wang, L., Zhou, J., Li, Y., Sun, F., Fu, G., et al. (2016). A worldwide evaluation of basin-scale evapotranspiration estimates against the water balance method. *Journal of Hydrology*, *538*, 82–95. https://doi.org/10.1016/j.jhydrol.2016.04.006

Liu, X., Liu, C., & Brutsaert, W. (2016). Regional evaporation estimates in the eastern monsoon region of China: Assessment of a nonlinear formulation of the complementary principle. *Water Resources Research*, *52*, 9511–9521. https://doi.org/10.1002/2016WR019340

Liu, Y., Pan, Z., Zhuang, Q., Miralles, D. G., Teuling, A. J., Zhang, T., et al. (2015). Agriculture intensifies soil moisture decline in Northern China. *Scientific Reports*, *5*(1), 11,261. https://doi.org/10.1038/srep11261

Long, D., Longuevergne, L., & Scanlon, B. R. (2014). Uncertainty in evapotranspiration from land surface modeling, remote sensing, and GRACE satellites. *Water Resources Research*, *50*, 1131–1151. https://doi.org/10.1002/2013WR014581

Ma, M., Wang, W., Jin, R., Huang, G., Zhang, Z., & Tan, J. (2008). WATER: Dataset of eddy covariance observations at the A'rou freeze/thaw observation station. Cold and Arid Regions Environmental and Engineering Research Institute, Chinese Academy of Sciences. https://doi.org/10.3972/water973.0282.db

Ma, N., Niu, G.-Y., Xia, Y., Cai, X., Zhang, Y., Ma, Y., & Fang, Y. (2017). A systematic evaluation of Noah-MP in simulating land-atmosphere energy, water, and carbon exchanges over the continental United States. *Journal of Geophysical Research: Atmospheres*, *122*, 12,245–12,268. https://doi.org/10.1002/2017JD027597

Ma, N., Szilagyi, J., Niu, G.-Y., Zhang, Y., Zhang, T., Wang, B., & Wu, Y. (2016). Evaporation variability of Nam Co Lake in the Tibetan Plateau and its role in recent rapid lake expansion. *Journal of Hydrology*, *537*, 27–35. https://doi.org/10.1016/j.jhydrol.2016.03.030

Ma, N., Zhang, Y., Szilagyi, J., Guo, Y., Zhai, J., & Gao, H. (2015). Evaluating the complementary relationship of evapotranspiration in the alpine steppe of the Tibetan Plateau. *Water Resources Research*, *51*, 1069–1083. https://doi.org/10.1002/2014WR015493

Ma, N., Zhang, Y., Xu, C.-Y., & Szilagyi, J. (2015). Modeling actual evapotranspiration with routine meteorological variables in the data-scarce region of the Tibetan Plateau: Comparisons and implications. *Journal of Geophysical Research: Biogeosciences*, *120*, 1638–1657. https://doi.org/10.1002/2015JG003006

Mao, Y., & Wang, K. (2017). Comparison of evapotranspiration estimates based on the surface water balance, modified Penman-Monteith model, and reanalysis data sets for continental China. *Journal of Geophysical Research: Atmospheres*, *122*, 3228–3244. https://doi.org/10.1002/2016JD026065

Mao, Y., Wang, K., Liu, X., & Liu, C. (2016). Water storage in reservoirs built from 1997 to 2014 significantly altered the calculated evapotranspiration trends over China. *Journal of Geophysical Research: Atmospheres*, *121*, 10,097–10,112. https://doi.org/10.1002/2016JD025447

Martens, B., Miralles, D. G., Lievens, H., van der Schalie, R., de Jeu, R. A. M., Fernández-Prieto, D., et al. (2017). GLEAM v3: Satellite-based land evaporation and root-zone soil moisture. *Geoscientific Model Development*, *10*(5), 1903–1925. https://doi.org/10.5194/gmd-10-1903-2017

Miralles, D. G., Jiménez, C., Jung, M., Michel, D., Ershadi, A., McCabe, M. F., et al. (2016). The WACMOS-ET project – part 2: Evaluation of global terrestrial evaporation data sets. *Hydrology and Earth System Sciences*, *20*(2), 823–842. https://doi.org/10.5194/hess-20-823-2016

Morton, F. I. (1983). Operational estimates of areal evapotranspiration and their significance to the science and practice of hydrology. *Journal of Hydrology*, *66*(1-4), 1–76. https://doi.org/10.1016/0022-1694(83)90177-4

Mueller, B., Hirschi, M., Jimenez, C., Ciais, P., Dirmeyer, P. A., Dolman, A. J., et al. (2013). Benchmark products for land evapotranspiration: LandFlux-EVAL multi-data set synthesis. *Hydrology and Earth System Sciences*, *17*(10), 3707–3720. https://doi.org/10.5194/hess-17-3707-2013

Mueller, B., Seneviratne, S. I., Jimenez, C., Corti, T., Hirschi, M., Balsamo, G., et al. (2011). Evaluation of global observations-based evapotranspiration datasets and IPCC AR4 simulations. *Geophysical Research Letters*, *38*, L06402. https://doi.org/10.1029/2010GL046230

Oleson, K., Lawrence, D. M., Bonan, G., & Drewniak, B. (2013). Technical description of version 4.5 of the Community Land Model (CLM). *NCAR/TN-503+STR NCAR Technical Note*, National Center for Atmospheric Research, Boulder, Colorado.

Or, D., & Lehmann (2019). Surface evaporative capacitance-how soil type and rainfall characteristics affect global scale surface evaporation. *Water Resources Research*, *55*, 519–539. https://doi.org/10.1029/2018WR024050

Ozdogan, M., & Salvucci, G. D. (2004). Irrigation-induced changes in potential evapotranspiration in southeastern Turkey: Test and application of Bouchet's complementary hypothesis. *Water Resources Research*, *40*, W04301. https://doi.org/10.1029/2003WR002822

Penman, H. L. (1948). Natural evaporation from open water, bare soil and grass. *Proceedings of the Royal Society A: Mathematical, Physical and Engineering Sciences*, *193*, 120–145. https://doi.org/10.1098/rspa.1948.0037

Peters-Lidard, C. D., Kumar, S. V., Mocko, D. M., & Tian, Y. (2011). Estimating evapotranspiration with land data assimilation systems. *Hydrological Processes*, *25*(26), 3979–3992. https://doi.org/10.1002/hyp.8387

Piao, S., Ciais, P., Huang, Y., Shen, Z., Peng, S., Li, J., et al. (2010). The impacts of climate change on water resources and agriculture in China. *Nature*, *467*(7311), 43–51. https://doi.org/10.1038/nature09364

Priestley, C. H. B., & Taylor, R. J. (1972). On the assessment of surface heat flux and evaporation using large-scale parameters. *Monthly Weather Review*, *100*(2), 81–92. https://doi.org/10.1175/1520-0493(1972)100<0081:OTAOSH>2.3.CO;2

Purdy, A. J., Fisher, J. B., Goulden, M. L., Colliander, A., Halverson, G., Tu, K., & Famiglietti, J. S. (2018). SMAP soil moisture improves global evapotranspiration. *Remote Sensing of Environment*, *219*, 1–14. https://doi.org/10.1016/j.rse.2018.09.023

Reichstein, M., Falge, E., Baldocchi, D., Papale, D., Aubinet, M., Berbigier, P., et al. (2005). On the separation of net ecosystem exchange into assimilation and ecosystem respiration: Review and improved algorithm. *Global Change Biology*, *11*(9), 1424–1439. https://doi.org/10.1111/j.1365-2486.2005.001002.x

Ren, G., Zhan, Y., Ren, Y., Chen, Y., Wang, T., Liu, Y., & Sun, X. (2015). Spatial and temporal patterns of precipitation variability over mainland China: I: Climatology. *Advances in Water Science*, *26*(3), 299–310.

Rodell, M., & Beaudoing, H. (2007). GLDAS CLM Land Surface Model L4 Monthly 1.0 x 1.0 degree V001, Greenbelt, Maryland, USA. Goddard Earth Sciences Data and Information Services Center (GES DISC). doi: 0.5067/0JNJQ8ZDZRBA

Rodell, M., Houser, P. R., Jambor, U., Gottschalck, J., Mitchell, K., Meng, C. J., et al. (2004). The global land data assimilation system. *Bulletin of the American Meteorological Society*, *85*(3), 381–394. https://doi.org/10.1175/bams-85-3-381

Román, M. O., Schaaf, C. B., Lewis, P., Gao, F., Anderson, G. P., Privette, J. L., et al. (2010). Assessing the coupling between surface albedo derived from MODIS and the fraction of diffuse skylight over spatially-characterized landscapes. *Remote Sensing of Environment*, *114*(4), 738–760. https://doi.org/10.1016/j.rse.2009.11.014

Shang, L., Zhang, Y., Lü, S., & Wang, S. (2015). Energy exchange of an alpine grassland on the eastern Qinghai-Tibetan Plateau. *Science Bulletin*, *60*(4), 435–446. https://doi.org/10.1007/s11434-014-0685-8

Shangguan, W., Dai, Y., Liu, B., Zhu, A., Duan, Q., Wu, L., et al. (2013). A China data set of soil properties for land surface modeling. *Journal of Advances in Modeling Earth Systems*, *5*, 212–224. https://doi.org/10.1002/jame.20026

Shen, M., Piao, S., Jeong, S. J., Zhou, L., Zeng, Z., Ciais, P., et al. (2015). Evaporative cooling over the Tibetan Plateau induced by vegetation growth. *Proceedings of the National Academy of Sciences of the United States of America*, *112*(30), 9299–9304. https://doi.org/10.1073/pnas.1504418112

Shi, P., Sun, X., Xu, L., Zhang, X., He, Y., Zhang, D., & Yu, G. (2006). Net ecosystem CO_2 exchange and controlling factors in a steppe—Kobresia meadow on the Tibetan Plateau. *Science in China Series D: Earth Sciences*, *49*(S2), 207–218. https://doi.org/10.1007/s11430-006-8207-4

Shukla, J., & Mintz, Y. (1982). Influence of land-surface evapotranspiration on the Earth's climate. *Science*, *215*(4539), 1498–1501. https://doi.org/10.1126/science.215.4539.1498

Sörensson, A. A., & Ruscica, R. C. (2018). Intercomparison and uncertainty assessment of nine evapotranspiration estimates over South America. *Water Resources Research*, *54*, 2891–2908. https://doi.org/10.1002/2017WR021682

Stoy, P. C., Mauder, M., Foken, T., Marcolla, B., Boegh, E., Ibrom, A., et al. (2013). A data-driven analysis of energy balance closure across FLUXNET research sites: The role of landscape scale heterogeneity. *Agricultural and Forest Meteorology*, *171-172*, 137–152. https://doi.org/10.1016/j.agrformet.2012.11.004

Su, T., Feng, T., & Feng, G. (2015). Evaporation variability under climate warming in five reanalyses and its association with pan evaporation over China. *Journal of Geophysical Research: Atmospheres*, *120*, 8080–8098. https://doi.org/10.1002/2014JD023040

Sun, S., Chen, B., Shao, Q., Chen, J., Liu, J., Zhang, X.-J., et al. (2017). Modeling evapotranspiration over China's landmass from 1979 to 2012 using multiple land surface models: Evaluations and analyses. *Journal of Hydrometeorology*, *18*(4), 1185–1203. https://doi.org/10.1175/jhm-d-16-0212.1

Szilagyi, J. (2014). Temperature corrections in the Priestley–Taylor equation of evaporation. *Journal of Hydrology*, *519*, 455–464. https://doi.org/10.1016/j.jhydrol.2014.07.040

Szilagyi, J. (2015). Complementary-relationship-based 30 year normals (1981–2010) of monthly latent heat fluxes across the contiguous U.S. *Water Resources Research*, *51*, 9367–9377. https://doi.org/10.1002/2015WR017693

Szilagyi, J. (2018a). A calibration-free, robust estimation of monthly land surface evapo-transpiration rates for continental-scale hydrology. *Hydrology Research*, *49*(3), 648–657. https://doi.org/10.2166/nh.2017.078

Szilagyi, J. (2018b). Anthropogenic hydrological cycle disturbance at a regional scale: State-wide evapotranspiration trends (1979–2015) across Nebraska, USA. *Journal of Hydrology*, *557*, 600–612. https://doi.org/10.1016/j.jhydrol.2017.12.062

Szilagyi, J., Crago, R., & Qualls, R. (2017). A calibration-free formulation of the complementary relationship of evaporation for continental-scale hydrology. *Journal of Geophysical Research: Atmospheres*, *122*, 264–278. https://doi.org/10.1002/2016JD025611

Szilagyi, J., & Jozsa, J. (2008). New findings about the complementary relationship-based evaporation estimation methods. *Journal of Hydrology*, *354*(1–4), 171–186. https://doi.org/10.1016/j.jhydrol.2008.03.008

Szilagyi, J., & Jozsa, J. (2018). Evapotranspiration trends (1979–2015) in the Central Valley of California, USA: Contrasting tendencies during 1981-2007. *Water Resources Research*, *54*, 5620–5635. https://doi.org/10.1029/2018WR022704

Szilagyi, J., & Schepers, A. (2014). Coupled heat and vapor transport: The thermostat effect of a freely evaporating land surface. *Geophysical Research Letters*, *41*, 435–441. https://doi.org/10.1002/2013gl058979

Tapley, B. D., Bettadpur, S., Ries, J. C., Thompson, P. F., & Watkins, M. M. (2004). GRACE measurements of mass variability in the Earth system. *Science*, *305*, 503–505.

Teuling, A. J., Hirschi, M., Ohmura, A., Wild, M., Reichstein, M., Ciais, P., et al. (2009). A regional perspective on trends in continental evaporation. *Geophysical Research Letters*, *36*, L02404. https://doi.org/10.1029/2008GL036584

Teuling, A. J., Seneviratne, S. I., Stöckli, R., Reichstein, M., Moors, E., Ciais, P., et al. (2010). Contrasting response of European forest and grassland energy exchange to heatwaves. *Nature Geoscience*, *3*(10), 722–727. https://doi.org/10.1038/NGEO950

Trambauer, P., Dutra, E., Maskey, S., Werner, M., Pappenberger, F., van Beek, L. P. H., & Uhlenbrook, S. (2014). Comparison of different evaporation estimates over the African continent. *Hydrology and Earth System Sciences*, *18*(1), 193–212. https://doi.org/10.5194/hess-18-193-2014

Velpuri, N. M., Senay, G. B., Singh, R. K., Bohms, S., & Verdin, J. P. (2013). A comprehensive evaluation of two MODIS evapotranspiration products over the conterminous United States: Using point and gridded FLUXNET and water balance ET. *Remote Sensing of Environment*, *139*, 35–49. https://doi.org/10.1016/j.rse.2013.07.013

Wan, Z. (2014). New refinements and validation of the collection-6 MODIS land-surface temperature/emissivity product. *Remote Sensing of Environment*, *140*, 36–45. https://doi.org/10.1016/j.rse.2013.08.027

Wang, G. Q., Zhang, J. Y., Jin, J. L., Pagano, T. C., Calow, R., Bao, Z. X., et al. (2012). Assessing water resources in China using PRECIS projections and a VIC model. *Hydrology and Earth System Sciences*, *16*(1), 231–240. https://doi.org/10.5194/hess-16-231-2012

Wang, K., & Dickinson, R. E. (2012). A review of global terrestrial evapotranspiration: Observation, modeling, climatology, and climatic variability. *Reviews of Geophysics*, *50*, RG2005. https://doi.org/10.1029/2011RG000373

Wang, X., Pang, G., & Yang, M. (2018). Precipitation over the Tibetan Plateau during recent decades: A review based on observations and simulations. *International Journal of Climatology*, *38*(3), 1116–1131. https://doi.org/10.1002/joc.5246

Wang, X., Yao, Y., Zhao, S., Jia, K., Zhang, X., Zhang, Y., et al. (2017). MODIS-based estimation of terrestrial latent heat flux over North America using three machine learning algorithms. *Remote Sensing*, *9*(12), 1326. https://doi.org/10.3390/rs9121326

Warren, J. M., Hanson, P. J., Iversen, C. M., Kumar, J., Walker, A. P., & Wullschleger, S. D. (2015). Root structural and functional dynamics in terrestrial biosphere models–evaluation and recommendations. *New Phytologist*, *205*(1), 59–78. https://doi.org/10.1111/nph.13034

Wen, X., Yu, G., Sun, X., Li, Q., Liu, Y., Zhang, L., et al. (2006). Soil moisture effect on the temperature dependence of ecosystem respiration in a subtropical Pinus plantation of southeastern China. *Agricultural and Forest Meteorology*, *137*(3–4), 166–175. https://doi.org/10.1016/j.agrformet.2006.02.005

Wilson, K., Goldstein, A., Falge, E., Aubinet, M., Baldocchi, D., Berbigier, P., et al. (2002). Energy balance closure at FLUXNET sites. *Agricultural and Forest Meteorology*, *113*(1-4), 223–243. https://doi.org/10.1016/S0168-1923(02)00109-0

Wu, C., Hu, B. X., Huang, G., & Zhang, H. (2017). Effects of climate and terrestrial storage on temporal variability of actual evapotranspiration. *Journal of Hydrology*, *549*, 388–403. https://doi.org/10.1016/j.jhydrol.2017.04.012

Wu, J., Jing, Y., Guan, D., Yang, H., Niu, L., Wang, A., et al. (2013). Controls of evapotranspiration during the short dry season in a temperate mixed forest in Northeast China. *Ecohydrology*, *6*, 775–782. https://doi.org/10.1002/eco.1299

Xu, C., & Singh, V. P. (2005). Evaluation of three complementary relationship evapotranspiration models by water balance approach to estimate actual regional evapotranspiration in different climatic regions. *Journal of Hydrology*, *308*(1-4), 105–121. https://doi.org/10.1016/j.jhydrol.2004.10.024

Xu, T., Guo, Z., Liu, S., He, X., Meng, Y., Xu, Z., et al. (2018). Evaluating different machine learning methods for upscaling evapotranspiration from flux towers to the regional scale. *Journal of Geophysical Research: Atmospheres*, *123*, 8674–8690. https://doi.org/10.1029/2018JD028447

Xu, T., Liang, S., & Liu, S. (2011). Estimating turbulent fluxes through assimilation of geostationary operational environmental satellites data using ensemble Kalman filter. *Journal of Geophysical Research*, *116*, D09109. https://doi.org/10.1029/2010JD015150

Yang, X., Yong, B., Yin, Y., & Zhang, Y. (2018). Spatio-temporal changes in evapotranspiration over China using GLEAM_V3.0a products (1980–2014). *Hydrology Research*, *49*(5), 1330–1348.

Yao, Y., Liang, S., Li, X., Zhang, Y., Chen, J., Jia, K., et al. (2017). Estimation of high-resolution terrestrial evapotranspiration from Landsat data using a simple Taylor skill fusion method. *Journal of Hydrology*, *553*, 508–526. https://doi.org/10.1016/j.jhydrol.2017.08.013

Yu, G. R., Wen, X.-F., Sun, X.-M., Tanner, B. D., Lee, X., & Chen, J.-Y. (2006). Overview of ChinaFLUX and evaluation of its eddy covariance measurement. *Agricultural and Forest Meteorology*, *137*(3–4), 125–137. https://doi.org/10.1016/j.agrformet.2006.02.011

Zeng, Z., Wang, T., Zhou, F., Ciais, P., Mao, J., Shi, X., & Piao, S. (2014). A worldwide analysis of spatiotemporal changes in water balance-based evapotranspiration from 1982 to 2009. *Journal of Geophysical Research: Atmospheres*, *119*, 1186–1202. https://doi.org/10.1002/2013JD020941

Zhang, H., Zhang, F., Zhang, G., Che, T., & Yan, W. (2018). How accurately can the air temperature lapse rate over the Tibetan Plateau be estimated from MODIS LSTs? *Journal of Geophysical Research: Atmospheres*, *123*, 3943–3960. https://doi.org/10.1002/2017JD028243

Zhang, L., Cheng, L., & Brutsaert, W. (2017). Estimation of land surface evaporation using a generalized nonlinear complementary relationship. *Journal of Geophysical Research: Atmospheres*, *122*, 1475–1487. https://doi.org/10.1002/2016JD025936

Zhang, Y., Pena-Arancibia, J. L., McVicar, T. R., Chiew, F. H., Vaze, J., Liu, C., et al. (2016). Multi-decadal trends in global terrestrial evapotranspiration and its components. *Scientific Reports*, *6*(1), 19,124. https://doi.org/10.1038/srep19124

Zhao, H., Fu, Y. H., Wang, X., Zhao, C., Zeng, Z., & Piao, S. (2016). Timing of rice maturity in China is affected more by transplanting date than by climate change. *Agricultural and Forest Meteorology*, *216*, 215–220. https://doi.org/10.1016/j.agrformet.2015.11.001

Zhao, L., Li, Y., Xu, S., Zhou, H., Gu, S., Yu, G., & Zhao, X. (2006). Diurnal, seasonal and annual variation in net ecosystem CO2 exchange of an alpine shrubland on Qinghai-Tibetan plateau. *Global Change Biology*, *12*(10), 1940–1953. https://doi.org/10.1111/j.1365-2486.2006.01197.x

Zhou, J., Wang, L., Zhang, Y., Guo, Y., Li, X., & Liu, W. (2015). Exploring the water storage changes in the largest lake (Selin Co) over the Tibetan plateau during 2003-2012 from a basin-wide hydrological modeling. *Water Resources Research*, *51*, 8060–8086. https://doi.org/10.1002/2014WR015846